eman ta zabal zazu
Universidad del País Vasco
Euskal Herriko Unibertsitatea
ZIENTZIA ETA TEKNOLOGIA FAKULTATEA
FACULTAD DE CIENCIA Y TECNOLOGÍA

Bachelor Final Thesis
Degree in Electronic Engineering

Automatic experimental characterization of a magnetic transport for low energy proton beams

Author:
Álvaro Bermejillo Seco

Supervisors:
Jorge Feuchtwanger Morales
Iñigo Arredondo Lopez de Guereñu

Leioa, 16th June 2021

Abstract

A computer controlled magnetic field measuring system designed for the magnetic characterization of a particle accelerator's Low Energy Beam Transport's (LEBT) solenoids is presented. The measuring system was assembled from commercially available components, mainly a Hall sensor and an XYZ positioner, whose selection and implementation is discussed. The measuring system was calibrated and tested on three different experiments. Then, the results of the solenoids' characterization and a comparison between simulated and measured fields are shown. The solenoids' measured field will be used to improve the beam dynamics simulations and through these, the best operation parameters for the LEBT can be found. An unexpected result of this work was that a fault in the manufacturing of the solenoids was discovered.

Resumen

Se presenta un sistema de medida de campo magnético controlado por ordenador para la caracterización magnética de los solenoides que forman el Transporte de Haz de Baja Energía (LEBT por sus siglas en inglés) de un acelerador de partículas. El sistema de medida se ha diseñado a partir de elementos disponibles comercialmente, principalmente un sensor Hall y un posicionador XYZ, cuya selección e implementación es discutida. El sistema de medida se calibra y prueba mediante 3 experimentos diferentes. A continuación, se muestran los resultados de la caracterización de los solenoides y una comparación entre los campos medidos y simulados. Las medidas del campo de los solenoides serán utilizadas para mejorar simulaciones de dinámica del haz y, a través de ellas, se podrán encontrar los parámetros de operación óptimos para el LEBT. Un resultado inesperado de este trabajo fue el descubrimiento de un error en la fabricación de los solenoides.

Laburpena

Ordenagailu bidez kontrolatutako eremu magnetikoen neurketa-sistema aurkezten da, partikula-azeleragailu baten Energia Baxuko Izpien Garraioa (LEBT, ingelesezko siglen arabera) osatzen duten solenoideen karakterizazio magnetikoa burutzeko. Neurketa-sistema komertzialki eskuragarri dauden elementuetan oinarrituz diseinatu da, Hall sentsore batetik eta XYZ mahai batetik nagusiki, zeinen hautaketa eta inplementazioa eztabaidatzen den. Neurketa-sistema hiru esperimentu desberdinen bidez kalibratu eta frogatu da. Jarraian, solenoideen karakterizazioaren emaitzak aurkezten dira, baita neurtutako eta simulatutako eremuen arteko konparazioa ere. Solenoideen eremuaren neurketa izpiaren dinamikaren simulazioak hobetzeko erabiliko dira eta horien bidez LEBTrako parametro optimoak aurkitu ahal izango dira. Lan hau burutzean ustegabeko akats bat aurkitu zen fabrikazioan.

Contents

1 Introduction **1**
- 1.1 The Linac-7 project . . . 1
- 1.2 Low Energy Beam Transport . . . 2
- 1.3 Solenoids . . . 3
- 1.4 Objectives . . . 4

2 Description of the system **6**
- 2.1 Key parameters for the design . . . 7
- 2.2 Components of the measuring system . . . 8
- 2.3 XYZ positioning table . . . 8

3 Sensor selection **10**
- 3.1 Criteria for sensor selection . . . 10
- 3.2 Comparison between preselected Hall sensors . . . 11
- 3.3 Selected Hall sensor . . . 13

4 System assembly **15**
- 4.1 XYZ positioning table adaptation . . . 15
- 4.2 Holding and wiring of the sensor . . . 15
- 4.3 Leveling of the system . . . 16
- 4.4 Set of the reference system . . . 17
- 4.5 Dimensional metrology and positioning operations . . . 19

5 Measuring system calibration **21**
- 5.1 Calibration of the Hall sensor . . . 21
- 5.2 Synchronization of movement and magnetic measurement . . . 23
- 5.3 Mapping of a magnetic quadrupole . . . 25

6 Solenoid measurements, data analysis and results **27**
- 6.1 Design of the experiment . . . 27
- 6.2 Calibration of the system . . . 28
- 6.3 Measurements . . . 30
  - 6.3.1 First iteration . . . 30
  - 6.3.2 Second iteration . . . 31
- 6.4 Further measurements . . . 34

7 Conclusions **35**
- 7.1 Future work . . . 35

1 Introduction

As of 2007 there were more than 24.000 particle accelerators in the world [1]. At the present time, there are around 35.000 [2]. Their applications range from the well known high energy accelerators for research, to medical applications such as radiotherapy or industrial applications such as ion implanters and surface modification [2]. This huge applicability encounters an impediment, the high complexity and costs of manufacturing such devices.

1.1 The Linac-7 project

In order to go beyond this obstacle, the University of the Basque Country, in cooperation with the industry sector of the Basque Country, launches in 2018 the Linac-7 project[1]. Its main objective is the design and manufacture of a new generation, compact, robust and economic low intensity linear proton accelerator. At the same time, this project fulfills many purposes:

1. Constitute an expert research team that grows designing and manufacturing components, and integrating them into a new generation particle accelerator.

2. Generate knowledge, in the local area, in the field of particle accelerators and promote the basque industry to a competitive level in the international frame of particle accelerators.

3. Maximize the commercial use of the research and experimentation results.

The project is still in its early stages, but big part of the design process has already been conducted. The project's name gives the first information about the systems characteristics. Linac stands for Linear Accelerator and 7 makes reference to 7 MeV, which is the final energy the particles will attain. In particular, Linac-7's objective is to design a compact, low current, linear proton accelerator. In order to achieve such a design, the system is split into different stages which are designed successively, from the source of the particles, to the final accelerating stage. Linac-7 is divided into 6 stages: 1) ECR (Electron Cyclotron Resonance) ion source, 2) LEBT (Low Energy Beam Transport), 3) RFQ (Radio Frequency Quadrupole), 4) MEBT (Medium Energy Beam Transport), 5) final accelerating element (not yet designed) and 6) beam stop (Figure 1).

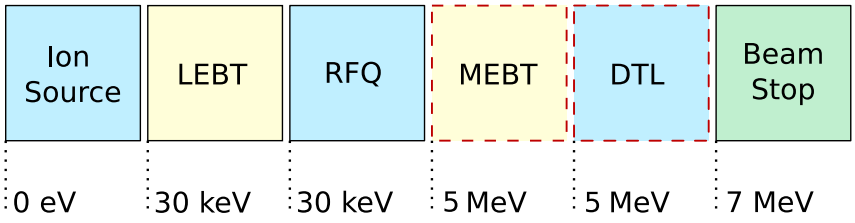

Figure 1: *Schematic description of the different stages of the Linac-7. The MEBT and the final accelerating stage, the Drift Tube Linac (DTL), are boxed in a red dashed line to indicate they have not yet been designed.*

[1]The information about the Linac-7 project is taken from internal reports. It is not available online. For consultation contact the author.

This text will focus its attention in the second of these stages: the Low Energy Beam Transport system.

1.2 Low Energy Beam Transport

The LEBT of any particle accelerator is the stage which receives the particle beam from the ion source and delivers it to the first acceleration stage. Its purpose is not to increase the energy of the particles, but rather to shape the beam and deliver it in a suitable form for acceleration.

The figure of merit to analyse the shape of a beam is the phase space diagram (y, p_y) for each coordinate, in the two transversal and the longitudinal axes. In practice, it is more usual to plot coordinates in the trace-space (y, y'), which replaces the momenta in favor of the angle between the analyzed axis and the propagation axis. This figure is closely related to a very important characteristic of the beam, the emittance[2] [3]. In Figure 2, it can be seen how a beam, before going through the LEBT, is essentially divergent, has positive angles in the positive coordinates and negative angles in the negative coordinates. On the contrary, after going through the LEBT, in Figure 2 the beam is essentially convergent, positive angles in the negative coordinates and vice versa. Thus, the beam has been focused in the y axis. Also, it is shown how the emittance, to some approximation the area enclosed by the particles in the trace-space, is conserved through the whole system.

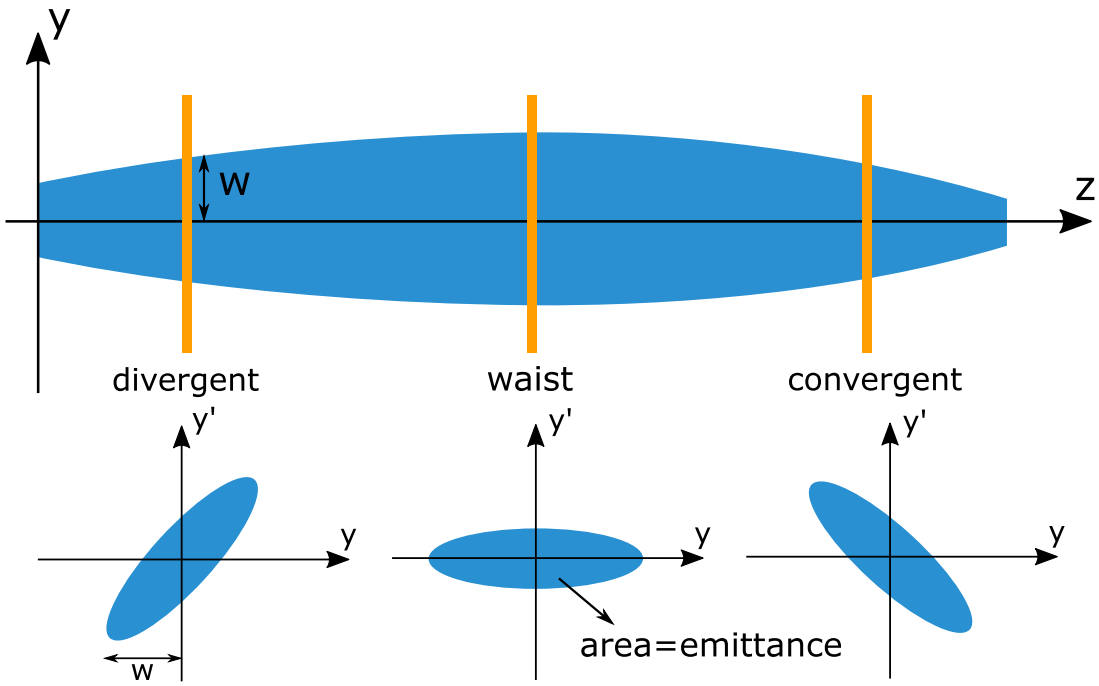

Figure 2: *Schematic evolution of the convergence of a beam going through a LEBT with the respective trace-space diagrams.*

LEBTs can be formed with elements which are classified into two types: electrostatic and magnetic.

[2]The emittance provides a quantitative basis to describe the quality of the beam. Low emittance is indicative of good quality.

1. **Electrostatic lenses.** These lenses modify the trajectories of the ions by means of electric fields. Some examples are the Einzel lens [4] (Figure 3a), a group of circular electrodes with alternate high and low voltages, and the Garbor lens [5], which takes advantage of the electric field generated by an electron cloud to focus the beam.

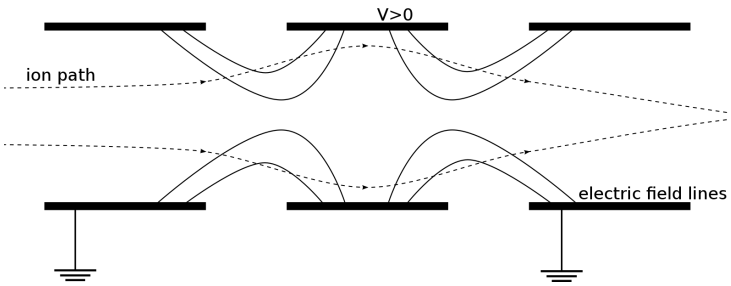

(a) *Example of a 3 electrode Einzel lens. (Source: Wikipedia, License: Creative Commons Attribution-ShareAlike 3.0 Unported License.)*

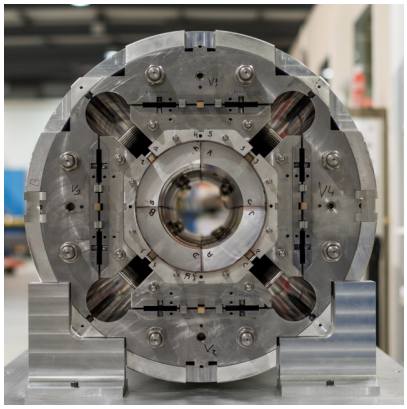

(b) *Example of a magnetic quadrupole. (Source: CERN.)*

Figure 3: *Types of lenses that form beam focusing systems.*

2. **Magnetic lenses.** These systems modify the characteristics of the ion beam by means of magnetic fields. Some examples are magnetic quadrupoles, formed either of permanent magnets or electromagnets (Figure 3b), and solenoids.

The Linac-7 design comprises a 4 electrode Einzel lens for the extraction of the ions from the ion source. Its aim is to give the particles from the ion source an initial acceleration and make an initial focusing of the beam. The design of this piece has a huge impact in the beam dynamics, because it determines the emittance of the beam, which then remains constant throughout the whole accelerator.

The LEBT's components are chosen following the required characteristics of the Linac-7 project. The more common option in the international installations is a configuration of two solenoids [6]. For the MEBT, conversely, it is more common to use magnetic quadrupoles due to their greater beam bending strength. With this choice the research group of the University of the Basque Country will be able to learn about both kinds of elements. Also, the solenoid implementation has some advantages for this particular case, it allows a more compact design and leaves space for beam diagnostics (i.e., a Faraday cup and a Pepperpot [7]). In summary, the choice of two solenoids for the LEBT matches the goals of the Linac-7 project presented before. The characterization of this system is what will be discussed in this text.

1.3 Solenoids

A solenoid is a type of electromagnet, a cylindrical coil which creates a magnetic field when carrying an electric current. The definition of a solenoid is simple, but their design can be complicated. As will be seen in Section 2 there are many factors involved in their proper functioning.

The magnetic flux density field of a solenoid is very characteristic. It is very constant in the inner region of the cylinder and decays rapidly out of it. The typical profile of the magnetic field along the axis of revolution of a solenoid is shown in Figure 4a and the contour of the field in a section perpendicular to the axis in Figure 4b. The contour shows how the field is more intense in the region near the conductors and reaches a minimum in a point in the center of the circle. The line formed by all those minimum field points from all the sections of the solenoid make up the magnetic axis.

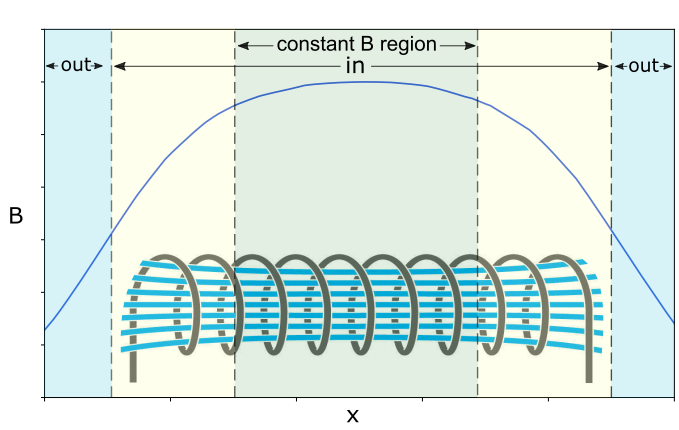

(a) *Example of the magnetic flux density amplitude along the axis of a solenoid. Three regions: outside of the solenoid, inside of the solenoid and in green the constant B region of the solenoid. Arbitrary units.*

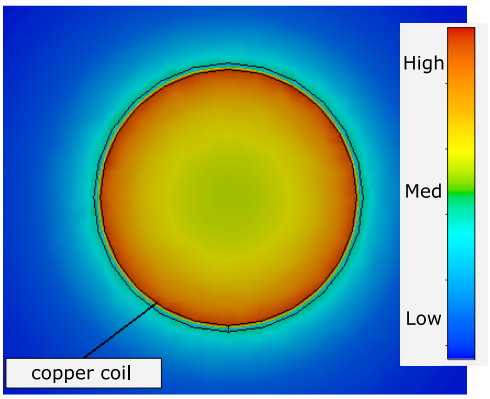

(b) *Example of the magnetic flux density contour in a section perpendicular to a solenoids axis. It can be appreciated how the field is weaker in the center, along the magnetic axis. Arbitrary units.*

Figure 4: *Characteristic magnetic field of a solenoid. Computed in Ansys AIM.*

1.4 Objectives

The purpose of this text is to explain and analyse in detail the magnetic characterization of the solenoids installed at the Linac-7's LEBT. In order to perform this characterization, the following measuring system is proposed: a three axis Hall probe attached to a computer controlled 3D positioning system. This system is capable of constructing a magnetic flux density field map.

The objective of this project is, then, to design and ensemble the 3D magnetic measuring system and measure the magnetic flux density field map of the solenoids that constitute the LEBT.

The interests in constructing such a map for the solenoids are mainly two:

1. **Find the magnetic axis of the solenoids.**

   As seen before in Figure 4b, in an ideal solenoid the magnetic axis is located in the center of the cylinder, it coincides with the mechanic axis of the solenoid. The mechanic axis of the solenoid is the geometric axis of revolution of the physical solenoid (Figure 5). Nevertheless, in real solenoids the mechanic and magnetic axis rarely match. Therefore, finding the magnetic axis is key for a correct functioning of the LEBT. The dynamics of the beam would be disturbed if it is not aligned with the solenoids' magnetic field; the focusing would be defective.

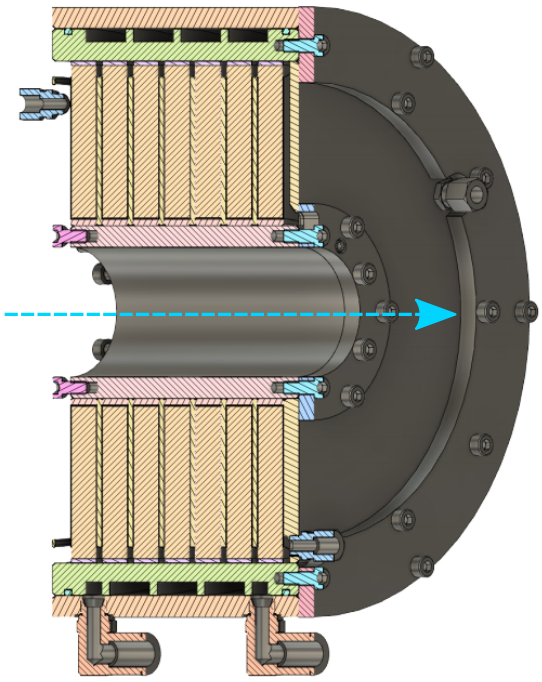

Figure 5: *CAD of the solenoid. The mechanic axis is drawn with a dashed blue line.*

2. **Study the differences between the simulated and the measured magnetic flux density field map.**

   Analysing the differences between the simulated and measured magnetic field will enable the use of the real parameters of the system in the beam transport simulations. The simulations with the measured magnetic field map are very useful in determining the operation parameters for the LEBT.

Finally, a GitHub repository will be created in order to make available the code necessary for the designed system's operation. Accessed: June 15, 2021. Available: https://github.com/abermejillo/BachelorThesis/tree/main/Electronic%20Engineering

2 Description of the system

The system to be characterized is the LEBT of the Linac-7. As said before, in this project the LEBT is composed of two solenoids. The CAD plane of a section of the LEBT is shown in Figure 6. The two solenoids are placed on each side of the vacuum chamber, which lays in the centre of the design. The horizontal tube, which goes through all the system, is called beam tube. The measurements of the magnetic field will be made inside the beam tube.

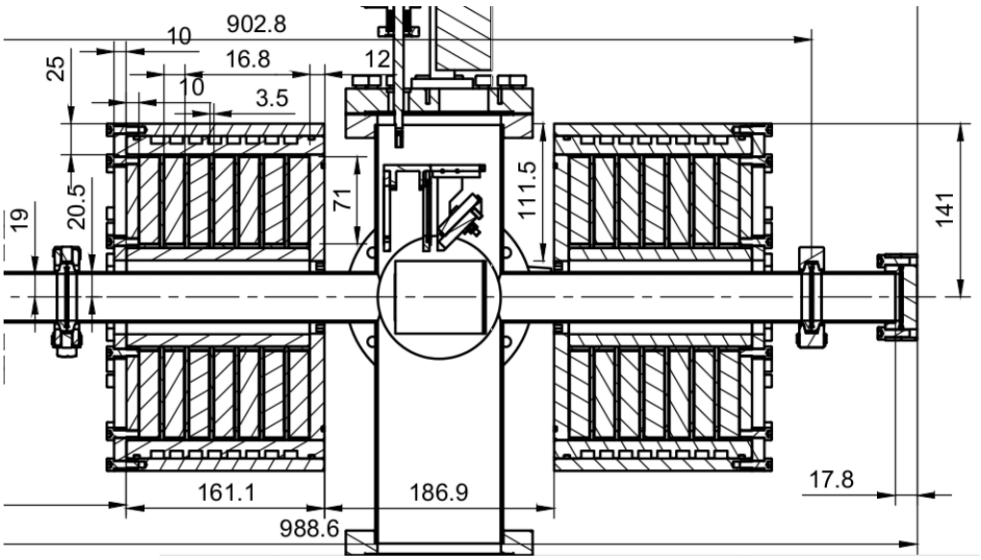

Figure 6: *CAD plan of a section of the LEBT. The two solenoids are set in the two sides of the vacuum chamber, in the centre. The division of the solenoids in 7 sub-coils can be appreciated here. Units in mm.*

As can be seen in Figure 7, the solenoid is assembled from several pieces. The beam tube, which is not part of the solenoid, are the walls of the region marked as 1. The rectangle marked as 2 is one of the 7 sub-coils. Those sections are where the copper wiring is placed and through where the current flows. And the region marked as number 3 is the steel casing.

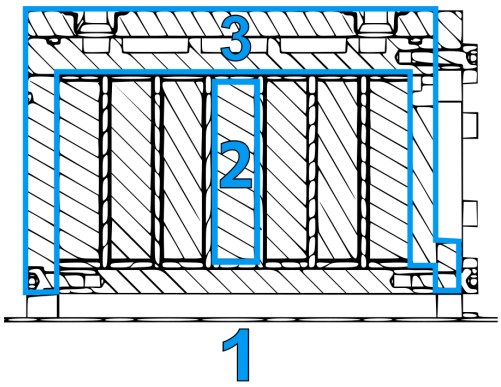

Figure 7: *Scheme of the solenoid where the different components can be differentiated. 1) Aluminium beam tube. 2) Copper wiring section. 3) High permeability ST-52 steel casing.*

The flow of current through the coils heats up the whole system. As the temperature of the structure rises, two main characteristics are affected. First, the conductivity of the copper decreases, and thus, maintaining the current requires more power. At the same time, the increase in temperature in the steel casing reduces its saturation magnetization. This, at the same time, reduces the magnetic flux density at the saturation condition ($B_s = \mu_0[M_s + H]$) [8].

These effects make necessary to include a refrigeration system for the solenoids. That is achieved with the division into sub-coils, which allows the solenoid to conduct heat through the material in between sub-coils to the exterior. In addition, a water refrigerating system is included through the steel casing.

A significative parameter of the sub-coils is the packing factor, a factor from 0 to 1 defined as the fraction of area occupied by the wiring. The lower the packing factor, less area is covered by cable. The packing factor of the solenoids manufactured for this LEBT is estimated to be 0.65. Nevertheless, the packing factor depends on many aspects (cable type and ability of the winder), and so the packing factor of each of the sub-coils and solenoid will be different.

2.1 Key parameters for the design

Some parameters of the solenoids are key for the design of the measuring instrument.

1. **Geometrical structure.** The diameter and length of the cylinder inside which the magnetic flux density is to be measured are important parameters. They present the limitations for the physical design. The inner diameter of the beam tube measures (38.00 ± 0.01) mm (Figure 6). In an ideal experiment, the magnetic flux density would be measured in the whole diameter, but due to the bulkiness of the sensor that is not possible.

2. **Magnetic flux density field.** To choose an appropriate magnetic field sensor, a magnetic flux field simulation is needed. In Figures 8 and 9, the magnetic flux density generated by the solenoid is simulated in Ansys AIM [9], a multiphysics simulator. From this simulation the range of the magnetic flux density can be extracted and used to choose the sensor accordingly. The nominal current used when operating the Linac-7 is approximately 8 A. Nevertheless, it is not necessary to perform the measurements in this configuration. It will be considered to set a lower current, which allows to use a more appropriate sensor.

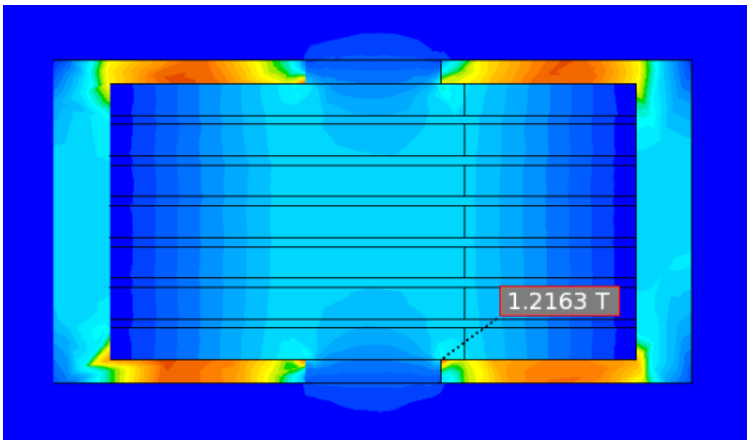

Figure 8: *Magnetic flux density contour simulated in Ansys AIM in a section of the solenoid for a current of 8.86 A. The highest magnetic flux density is found inside the steel casing. In the region inside the solenoid (vertical light region in the center), the magnetic flux density has a value of approximately 350 mT.*

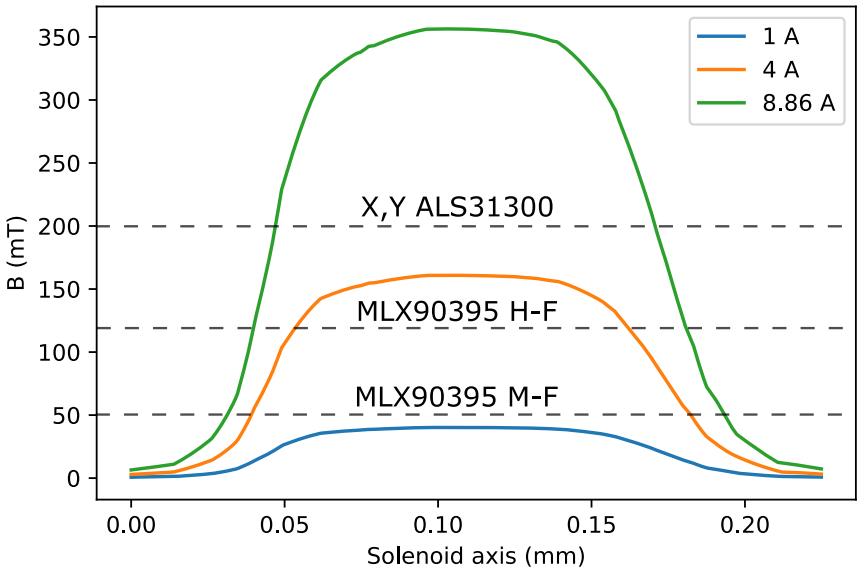

Figure 9: *Magnetic flux density (B) profile simulated in Ansys along the axis of the solenoid for 3 different currents. The dashed lines mark the range limit of the 3 preselected sensors, which will be relevant in Section 3.*

2.2 Components of the measuring system

With this information about the geometry of the system and the nature of the measurements to be made, a design of the measuring system is developed.

To map the magnetic flux density on the cylinder volume inside the solenoid two things are needed: a magnetic flux density sensor and the ability to position the sensor with precision in different points of space. The magnetic flux density sensor is implemented with a Hall sensor [14], and the positioning in space is performed with an XYZ positioning table. The selection of the Hall sensor is developed in Section 3, and the selected XYZ positioning table is presenter hereafter.

2.3 XYZ positioning table

An XYZ positioner is made up of three independent linear positioners oriented normal to each other. Each linear positioner consists of a mechanical system that conveys rotatory to linear motion. The rotatory motion is provided by a motor, which can be controlled. The control system traduces a linear motion command into the required rotation of the motor to achieve said displacement.

For this project the OpenBuilds Minimill [10] (Figure 10a) is used as the XYZ positioner. In this system, lead screws in the linear guides are driven by steppermotors. The system is controlled by the OpenBuilds Blackbox [11] (Figure 10b), that includes the drivers for the steppermotors and a microcontroller that interprets the commands and sends the appropriate signals to the stepper motors.

(a) *OpenBuilds Minimill, the system's positioning structure, steppers and drivers [10].*

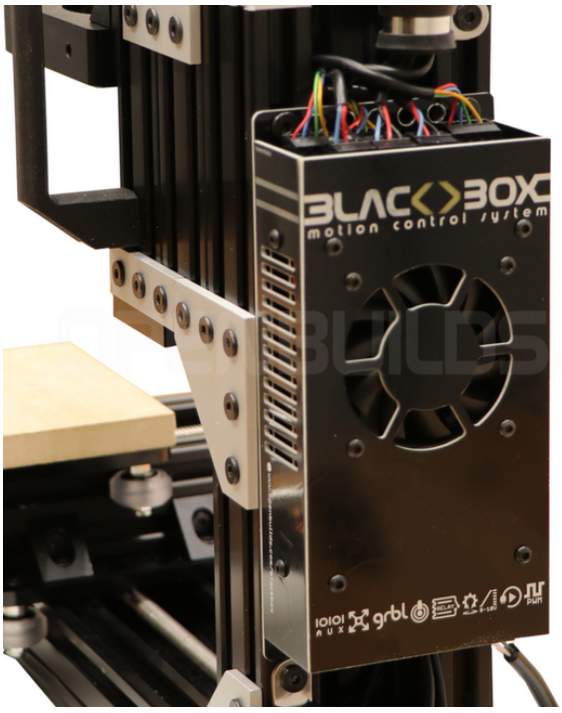

(b) *OpenBuilds Blackbox, the system's microcontroller [11].*

Figure 10: *Components of the positioning XYZ table.*

One of the main advantages of the system is that it is open source, which allows to have access to every feature and modify it to fit this project's purposes. The most defining characteristics of the Minimill are the dimensions of each axis: X 120 mm × Y 180 mm × Z 80 mm. The longest, the Y axis, is longer than the length of the solenoid; it will be the axis aligned with the mechanic axis of the solenoid.

The Blackbox is the microcontroller, the motion control system. The communication between a computer and the Blackbox works via the USB and it runs Grbl 1.1 [12]. Grbl is the free software for motion control of CNC (Computer Numeric Control) which sends the adequate signals to the steppers based in the received commands. Those commands are written in the G-code programming language, based on the standard ISO 6983-1:2009 [13]. An example of a G-code line is "G91 G21 G01 Z-10 F200", which means: (G91) incremental positioning (G21) length units to mm (G01) linear movement (Z-10) 10 mm in the Z negative direction (F200) with a Feed Rate of 200 mm per minute. Every action of the system has to be translated into these simple commands and sent to the Blackbox through the serial port.

The Blackbox is possibly the most sensible component of the system. It has been replaced twice in the course of the project. Apart from this, the whole system has proved to be precise during all the tests performed during the project. These tests will be shown in Section 5.

3 Sensor selection

One of the main design tasks for this project it the selection of a magnetic flux density sensor. The sensors for static magnetic fields are based on the Hall effect [14]. Hall effect sensors are very common due to their numerous applications in industry (e.g., joysticks, position sensors or compasses). Associated with this applicability comes a wide catalogue from which the sensor can be selected. With that purpose a list of criteria is established.

3.1 Criteria for sensor selection

The first step towards defining a list criteria is analysing, through simulation, the solenoids' magnetic field. The simulation is performed in Ansys AIM, an engineering multiphysics simulator. To obtain it, a 3D model is created according to the geometry specified in Figure 6. Then the appropriate material characteristics are assigned to each element: copper for the 7 sub-coils, steel ST-52 for the casing, and air for the surroundings. Because of the static nature of the field in this system, all the components of the LEBT which are not the sub-coils or the casing are non magnetic steel or aluminium, which have the same magnetic permeability as the air [15]. In addition, Ansys AIM allows to introduce the B-H curve for the ST-52 (Figure 11) which improves the magnetic simulation.

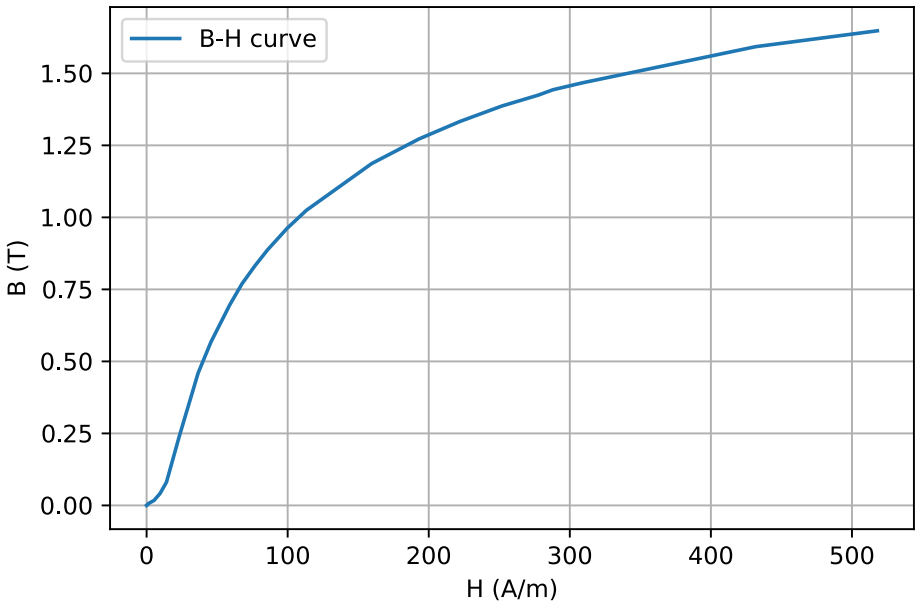

Figure 11: *Experimental measurement of the B-H curve for steel ST-52. This curve is inserted in Ansys AIM to perform the magnetic simulation of the solenoid.*

The results of those simulations are shown in Section 2 in Figures 8 and 9. With this information the criteria can now be given.

1. **3D Hall sensor.** The nature of magnetic fields is a three dimensional vector field. And, although the magnetic field inside some of the region of the solenoid is

very constant and unidirectional, that does not mean that we are not interested in analysing the magnetic field in the outer regions of the solenoid. In those regions, the magnetic field closes through the steel casing and it is of interest to measure how the magnetic flux density lines behave at the ends of the solenoid. To capture that behaviour B is measured in the 3 coordinates of space.

2. **Compatibility with Arduino.** An Arduino microcontroller is going to be used to establish the communication between the sensor and a computer, where the data will be processed. Sensors with I^2C serial communication are not uncommon, and Arduino supports that protocol through the specific SCL(clock) and SDA(data) pins.

3. **Size.** To measure in most of the diameter inside the beam tube it is needed to reduce the size of the sensor as much as possible. The sensor will be placed in the tip of an aluminium bar with a section of 10 mm $\times$ 10 mm. Therefore, the implemented sensor needs to fit into those dimensions. For this reason, the sensor will be acquired as a chip, unassembled, in order to have freedom to solder and install the circuit in the most suitable manner.

4. **Magnetic flux density range.** This parameter is less constraining, because the current that flows through the solenoid can be changed. The upper limit will be given by the highest magnetic flux density in the simulation with the intensity to be used when focusing the beam (around 8 A). The lower limit is 0 independently of the current, because the magnetic field decays rapidly outside the solenoid (Figure 9).

5. **Sensitivity.** It will be an important parameter for which there is no specific criteria. It will have to be checked that the sensitivity is high enough to measure a curve like the one in Figure 9. Depending on the range of the sensor a different current will be used and the sensitivity will need to be adequate.

6. **Output data rate (ODR).** In order to cancel most of the noise of the sensor, the measurement in each point of space will be the average of some number of individual measurements. The process of finding an adequate number of measurements will be made in Section 5. The ODR is then important to control the time it takes to perform the whole characterization of the solenoid. That time will depend on the ODR, the number of measurements per position and the number of positions. It will also be affected by the time it takes to move the XYZ positioning table from one point to the next. All in all, the higher the ODR the better.

3.2 Comparison between preselected Hall sensors

Three different 3D Hall sensors were preselected as suitable for the design: ALS31300 JOY [16], MLX90395 High-Field [17] and MLX90395 Medium-Field [17]. Table 1 shows their principal characteristics.

Table 1: *Principal characteristics of the preselected sensors [16] [17]. All of them are sensible in 3 axes (X,Y and Z) and compatible with Arduino through I^2C communication.*

	ALS31300	MLX90395 High-Field	MLX90395 Medium-Field
Range	X,Y ± 200 mT Z ± 800 mT	± 120 mT	± 50 mT
Sensitivity	X,Y 0.1 mT/LSB_{12} Z 0.4 mT/LSB_{12}	7.14 μT/LSB_{16}	2.5 μT/LSB_{16}
Noise RMS	X,Y 0.3 mT Z 0.4 mT	1.08 mT (T=35 ºC)	0.275 mT (T=35 ºC)
ODR	2 kHz	1.5 kHz	1.5 kHz
Size	10 contact DFN 3×3×0.8mm	SOIC-8 6.20×4.98×1.72mm	SOIC-8 6.20×4.98×1.72mm

These 3 Hall sensors are all valid. ALS31300 could be used to measure the magnetic field with a current of around 8 A as long as the Z axis of the sensor is aligned with the axis of the solenoid, the direction in which the highest magnetic flux density in given. This option was tried, but gave bad results.

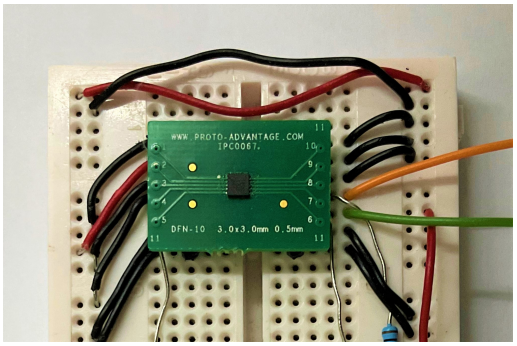

Figure 12: *ALS31300 chip soldered into a IPC0067.*

The ALS31300 Hall sensor was soldered into a DFN 10 to DIP-14 SMT adapter (Figure 12) with soldering paste following a specific heat curve in a temperature controlled oven [18]. The measurements made with an evaluation prototype for this sensor are shown in Figure 13. The X and Y axes were unresponsive and the Z axis had a much higher noise than what the data sheet reported. As the company which manufactures the sensors gives no support to individuals, the problem could not be solved and this option was discarded.

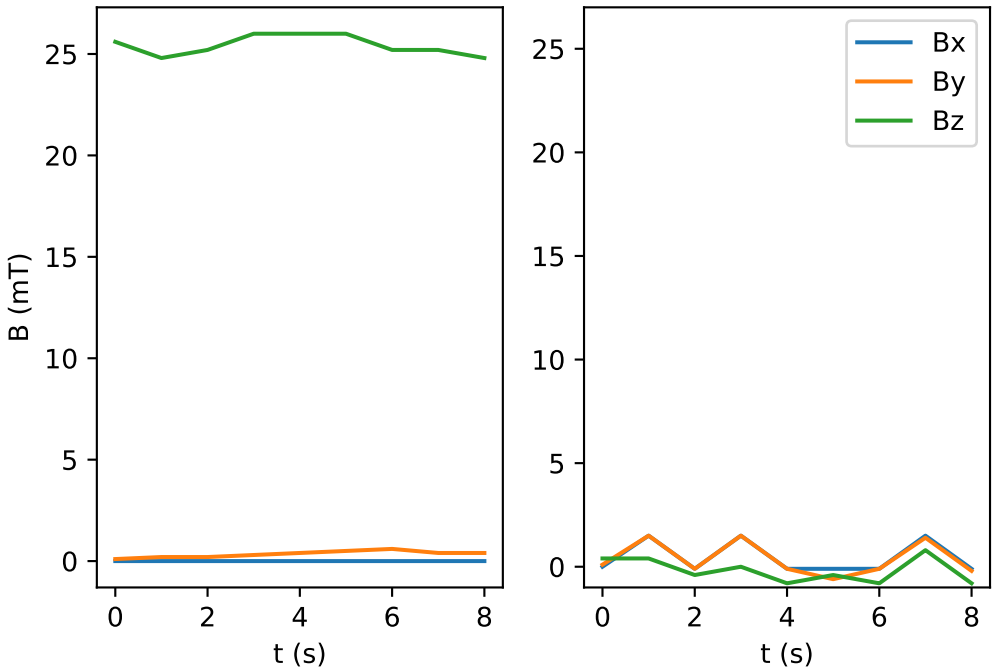

Figure 13: *Typical measurements of the magnetic field of a NdFeB N45 magnetic cylinder with the ALS31300 Hall sensor. On the left: The permanent magnet is held along the Z axis. On the right: Same magnet held along the X axis. Along this axis the sensor is unresponsive. Holding the magnet along the Y axis gives the same result as the X axis.*

3.3 Selected Hall sensor

Neither of the two MLX90395 are valid to measure with a current around 8 A, which is a downside. However, their analog-digital converter (ADC) is of 16 bits [17] (compared to the 12 bit ADC of the ALS31300 [16]), so some accuracy is won. From the two MLX90395, both are equally valid provided that the current is adjusted so that the magnetic flux density matches the range of the sensor. Finally, prioritizing precision over range, the selected sensor was the **MLX90395 Medium-Field**.

To implement the circuit a SOIC-8 to DIP-8 SMT Adapter was used, shown in Figure 14. The circuit, soldered onto the PCB, is shown in Figure 15a. The SOIC-8 is easily soldered with a tin solder, so the heating process with soldering paste mentioned before is not needed.

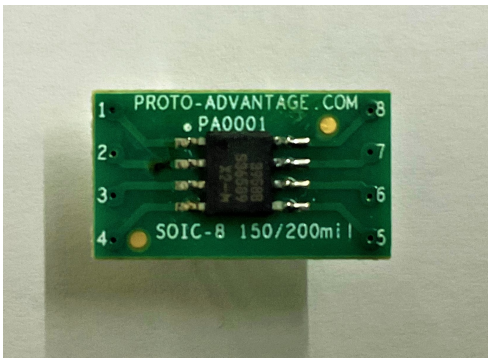

Figure 14: *MLX90395 chip soldered into a DIP-8 SMT Adapter.*

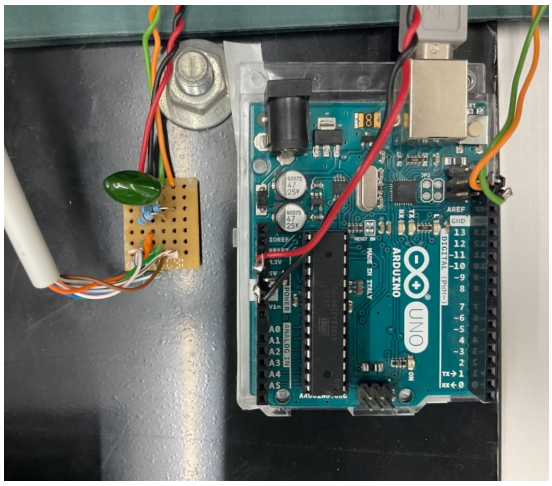

(a) *Soldered sensor circuit into a PCB. The wires coming from the lower part of the PCB are the connections to the sensor's pins. The sensor chip is located in the other end of the shielded cable. The setup will become clearer in Section 4.*

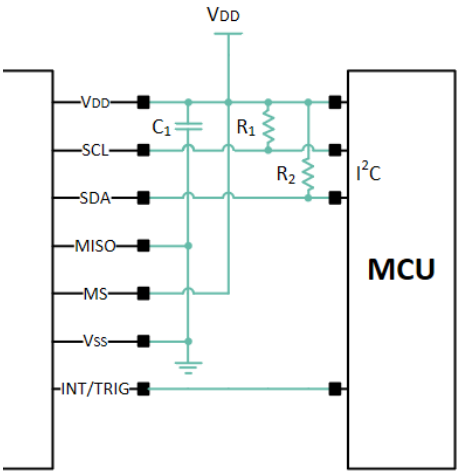

(b) *Scheme of the circuit: MCU is the microcontroller unit (Arduino), I^2C pull-up resistors, bypass capacitor to reduce AC noise from the source, V_{DD}=3.3V and GND. The INT/TRIG pin is not used.*

Figure 15: *Circuit of the MLX30395 Hall sensor.*

To sum up, after the analysis of some 3D Hall sensors in the market, the selected one is MLX30395 Medium-Field. This sensor allows to measure the magnetic flux density in the solenoid with a current of 1.0 A. It communicates with Arduino through the I^2C protocol (Figure 15b), which allows an easy acquisition of the data in the PC with Arduino code.

4 System assembly

In this section the assembly of the final measuring system is outlined.

4.1 XYZ positioning table adaptation

The base of the system is the XYZ positioning table based in the OpenBuilds MiniMill. This machine is meant for milling, but making some adjustments it can be adapted for this project's purposes. Picture the usual XYZ coordinate system, with Z in the vertical axis. It can be seen in Figure 10a that if the sensor is placed in the vertical axis, it is uncoupled from the X and Y axes. This means that moving the X and Y axes does not move the sensor. However, turning around the platform of the XY axes and fixing it to the table couples all axes. With the platform fixed to the table, when the motors try to move the platform they move the whole machine instead. That configuration can be seen in Figure 16 and compared to the previous in Figure 10a.

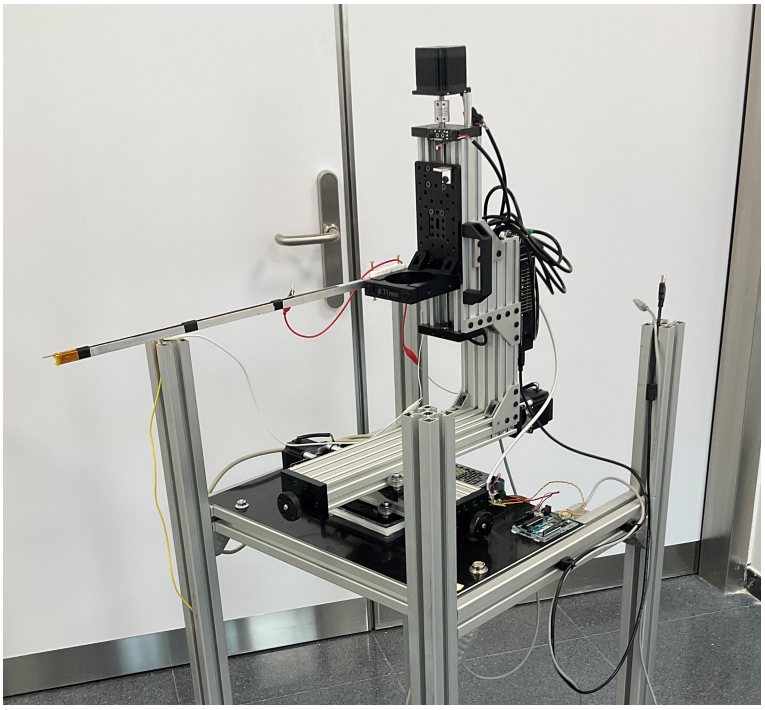

Figure 16: *Adapted Minimill with coupled XYZ axes. The milling platform seen in Figure 10a is fixed to the black surface.*

4.2 Holding and wiring of the sensor

The sensor is placed in a 600 mm × 10 mm × 10 mm aluminium bar. The tip of the bar was milled so as to place the sensor approximately in the center of the bar. This bar is the piece, that attached to the black moving piece in the Z axis (Figure 16) will move the sensor from point to point in space and will enable to access small cylindrical wholes. Through the interior of this aluminium bar goes a shielded cable which connects the sensor with the PCB shown in Figure 15a. With the shielding, the digital signals of the sensor (I^2C's SCL and SDA) will not be perturbed when moving through any

magnetic field. Also, the individual cables inside the shielded cable are braided to reduce the possible electromagnetic interferences.

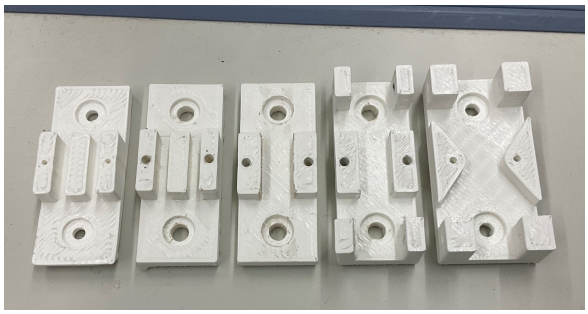

(a) *Versioning of the 3D printed piece which fixes the sensor's arm to the Minimill. Chronologically from left to right.*

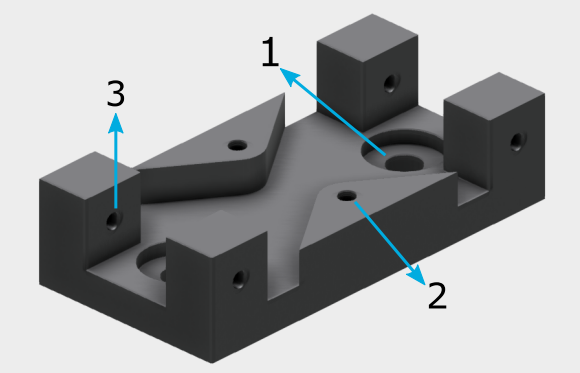

(b) *Model of the definitive version of the 3D printed piece.*

Figure 17: *3D printed piece designed for the holding of the Hall sensor arm.*

To fix the aluminium bar to the Minimill a 3D printed piece was designed in Fusion360 [19] (Figure 17b). It went through a versioning process shown in Figure 17a. The one shown in Figure 17b is the fifth and definitive version. The first pieces (Figure 17a) were designed for another sensor holding, other than the aluminium bar. That first model was designed with a plastic bar, which was discarded because it was not rigid enough and presented too much vibration with the XYZ positioner movements. The latter versions added new functionalities, which are listed hereafter, or improved already existing ones. The 3D printed piece has three functionalities: it fixes itself to the Minimill with two screws through 1 (Figure 17b), the bar is fixed to the piece with another two screws through 2 (Figure 17b) with an aluminium plate, and with the 4 screws in 3 (Figure 17b) the tilt of the bar in the YZ plane is regulated by independently changing the height of 2 different points of the bar.

4.3 Leveling of the system

This functionality is of uttermost importance for the measurements. It is essential that the sensor moves parallel to the solenoid axis. Any deviation in the leveling of the components of the systems would produce an error in the measured positions of the solenoid. If a movement is started with the tip of the aluminium bar in the center of a section of an end of the solenoid, and the components are not parallel, when the machine reaches the other end of the solenoid the tip would not be in the center. Thus, the positions of the measurements would not correlate with the real position inside the solenoid. In principle, the two ways to solve the problem are: to align all the components between themselves or to measure the tilt and correct the measured position in post-processing. However, this second approach is inefficient, because the tilt of the bar would reduce the allowed travel of the machine.

To ensure that the whole system is aligned there are 3 requirements: the XY plane of the 3D machine, the aluminium bar which holds the sensor, and the sensor itself need to be parallel to the mechanical axis of the solenoid. The easiest reference to adjust the tilt

of all the components is gravity. With a bubble level tool and a laser level it is guaranteed that all components of the measuring system and the measured system are perpendicular to the gravitational acceleration.

The whole machine is set on top of an aluminium structure (Figure 16) that allows to change its height and make small corrections to its tilt. The tilt of the aluminium bar can be corrected with the mechanism embedded in the designed 3D piece and the tilt of the sensor has to be taken into account when fixing it to the aluminium bar.

4.4 Set of the reference system

Previously it has been discussed how an error in the leveling of the system can affect the correlation between the measured positions and the real positions inside the solenoid. This correlation only exists if there is a reference system in the first place. The reference system is needed to give the 3D movement machine a starting point and relate machine coordinates to positions in real space. To achieve that, a touch probe device is set up.

The probe is supported in the Openbuilds Minimill and has specific commands in Grbl. The working principle is simple. First, a non magnetic conductor tip is placed at the end of the aluminium bar. This piece of conducting metal is connected to a signal produced in the micro-controller of the Minimill. Secondly, the front end of the beam tube is connected to logical ground (GND in the micro-controller). With these connections, when the signal tip makes contact with GND the microcontroller detects it (Figure 18). It is important that the conductor tip is non magnetic or else it would disturb the magnetic field in a region very near to the Hall sensor.

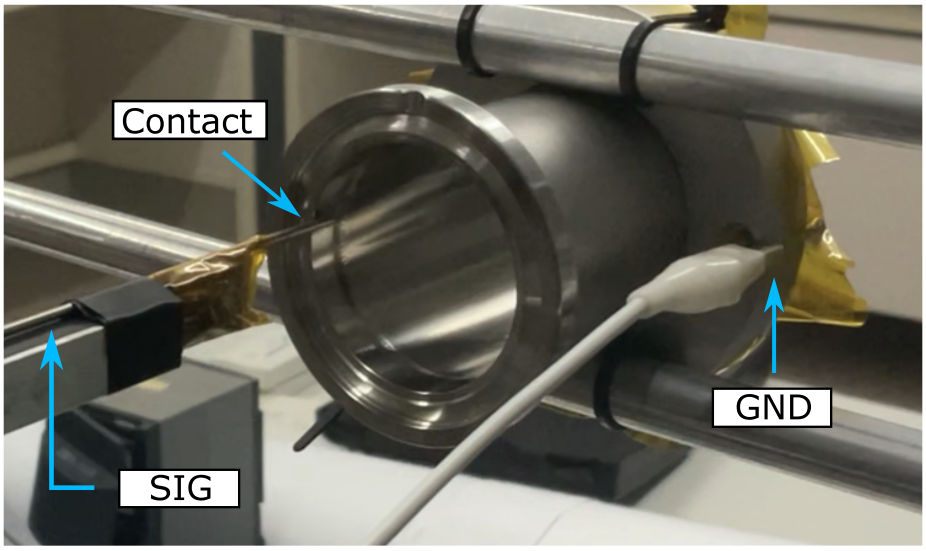

Figure 18: *Example of the probing system. The probe can be seen making contact with the left side of a piece of the accelerator, that is, setting the signal (SIG) to logical ground (GND).*

With this functionality it is now possible to design an algorithm to find the center of a conductor cylinder in the front end of the solenoid. The steps are the following:

1. Starting from approximately the center of the cylinder it moves in the X axis until it touches the wall, and records its position.

2. From that position it moves in the opposite direction until it touches the other wall and records its position. With the two positions it computes the centre of the cylinder section in the X axis: $X_{centre} = (X_{right} - X_{left})/2$.

3. From the center in the X axis it moves in the positive Z axis until it touches the solenoid, and records its position.

4. From that position it moves in the negative Z direction and records the position of the solenoid wall. As before, it computes the center in the Z axis: $Z_{centre} = (Z_{top} - Z_{bottom})/2$.

5. If the result is not sufficiently accurate, the process is repeated. Sometimes not starting near the center produces tangential forces on the probe leading to inaccuracies, that is why repeating the process from a better approximation of the center improves the result.

6. Finally, to find the 0 position in the Y axis, the machine moves out of the solenoid in the Y direction, and then radially until it is beyond the diameter of the beam tube. From there it moves towards the solenoid's front end until it makes contact and records the position. That position marks the start of the solenoid, Y_0.

The ending position X_{center}, Y_0, Z_{center} is the center of the probed cylinder in one of its end faces. At the end of this algorithm, the tip of the probing system is placed at that point in space. A last step is needed to place the sensitive spot of the Hall sensor in that same point; the vector which goes from the sensitive spot to the tip of the probing system needs to be measured.

Because of the irregularity of the shape of the tip, the measuring of that distance with a caliper is remarkably difficult. Therefore, a different method is followed. A reference distance is taken; the diameter of the probing system's tip is measured with a caliper $\phi = (1.54 \pm 0.01)$ mm. Then two photos of the head of the aluminium bar are taken with a USB microscope (Figure 19). Consecutively, a software named ImageJ [20] allows to establish, in those photos, a relation between the number of pixels between 2 points and a given distance, in this case the diameter of the probing system's tip. Once the distance per pixel is calibrated any distance can be extracted from the photos. In addition, the location of the sensitive spot within the Hall sensor is specified in the data sheet [17].

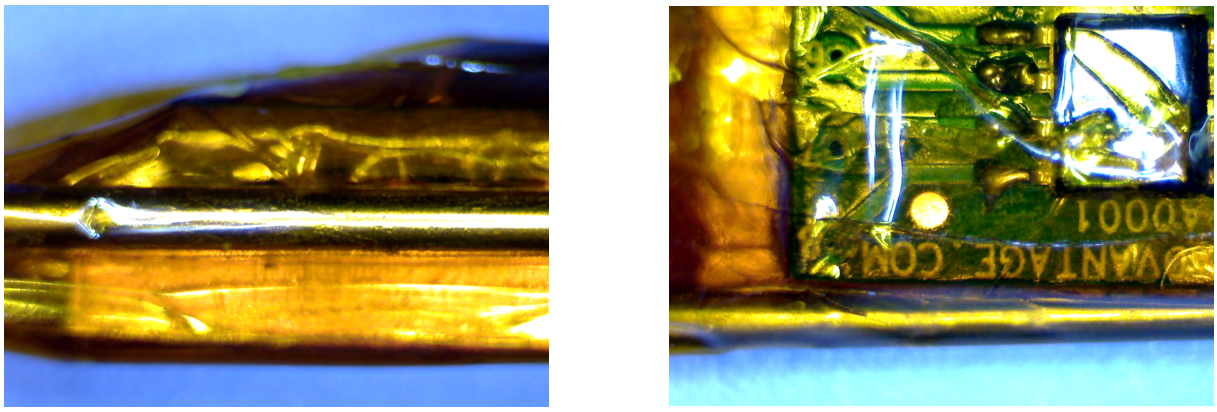

Figure 19: *Photos of the tip of the aluminium bar taken with the USB microscope.*

Following this method the sought vector is:

$$\vec{V}_{\text{displacement}} = (-3.53, -33.15,\ 6.23) \pm 0.01 \text{ mm}$$

After probing and moving the system the distance $\vec{V}_{\text{displacement}}$ the sensitive spot of the Hall sensor is in the center of the cylinder with a precision of 0.1 mm, the precision of the Openbuilds Minimill.

The error in the final position that the probing algorithm finds could be greater that 0.1 mm due to the delay in detecting that the probe makes contact with the wall of the beam tube. However, due to the symmetry of the movements that error is cancelled out in the X and Z axes. The Y axis does not present that symmetry, but the probing is made perpendicular to the surface of the beam tube. There is, hence, no possibility for the probe to bend and increase the error. Besides, the error in calculating the $\vec{V}_{\text{displacement}}$ is lower than the precision of the machine. The uncertainty in the reference measure is of 0.01 mm (the precision of the caliper) and the quality of the images is very high, so the uncertainty in pixels, which can be estimated to be between 5 and 10 pixels, results in a position uncertainty lower than 0.1 mm. In conclusion, the limitation of the setting of the reference system is given by the movement precision of the steppers of the Minimill.

4.5 Dimensional metrology and positioning operations

Having presented some of the sources of error that the positioning of the Hall sensor introduces to the construction of a magnetic field map, it is of interest, before making any measurement, to remark some general aspects of the measuring system and error sources.

Dimensional metrology and positioning operations are used in many fields of particle accelerator projects [21]. It includes the techniques and instrumentation to measure both dimension of an object and the relative position between several objects (alignment). Dimensional metrology tools are split into two categories: sensors that deliver the measure of physical dimensions and mechanical tools that deliver the positions.

A third component has to be taken into account if greater precision wants to be reached: time dependence of the measures. The solenoids of the Linac-7's LEBT are current controlled, which means that the current remains very stable at the desired value, and have a refrigeration system which regulates the temperature. Thus, the system can be regarded as time invariant, and time dependence does not play a major role.

There are three categories of errors in the domain of measure [21].

1. Random errors: for sensors, they correspond to microscopic effects coming from the electronic devices.

2. Bias errors: a bias can exist in the result of a measurement procedure. For example, the zero value of the Hall sensor is not well known, there is an offset. This error will be palliated with the first experiment performed in the next section, Section 5.1.

3. Errors depending on external sources: temperature variations or mechanical vibrations are typical examples of this sources.

Random errors can be greatly reduced by averaging processes and some external errors such as temperature variations can be reduced by reducing the time duration of the measurement. However, bias errors are systematic and need to be individually detected and accounted for.

A good method to systematically avoid bias errors is to keep the metrology loop as short as possible. The metrology loop is the succession of mechanical parts and sensors that a system requires to operate and measure. The metrology loop of this project's measuring system is composed of:

1. Mechanical parts: the aluminium structure in which the Minimill is fixed, the rails of the XYZ positioning table, the 3D printed piece which holds the aluminium bar of the sensor, the aluminium bar itself and the Hall sensor, understood as a piece which has to be properly aligned.

2. Sensors: the internal position and velocity measuring systems of the XYZ positioning table's stepper motors, the probing system which allows to set a reference system and all the external instruments which are used to calibrate the system (i.e. the caliper, the bubble level tool and the laser level).

The alignment of all the mechanical parts has a direct effect in the correct positioning of the moving system, and the precision of that alignment is set with the accuracy of the sensors employed.

5 Measuring system calibration

An indispensable previous step to the measurement of the magnetic flux density in the solenoids of the LEBT is the calibration of the system. That is, obtaining a transfer function for the Hall sensor and finding the best configuration for the movement of the XYZ positioning table. For this purpose three different experiments will be performed:

1. **Calibration of the Hall sensor.** The measurements of the MLX90395 sensor Hall will be compared by measuring the known magnetic flux density of a solenoid in the vibrating sample magnetometer from the general services of magnetic measurements of the Science and Technology Faculty of the University of the Basque Country.

2. **Synchronization of movement and magnetic measurement.** By this experiment, the first trial of synchronizing the movement of the XYZ positioning table and the Hall sensor acquisitions is carried out. The magnetic field is measured along a line equidistant to both poles of a magnetic dipole and compared with a simulation performed in FEMM (Finite Element Method Magnetic) [22].

3. **Mapping of a magnetic quadrupole.** This experiment shows the limitations the bulkiness of the sensor introduces to measure the magnetic field in the edges of the interior of a cylinder. To do so, the field of a magnetic quadrupole is measured in a circular area.

5.1 Calibration of the Hall sensor

The MLX90395 Hall sensor performs internally the transformation from voltage (Hall voltage [14]) to magnetic flux density through a software implemented transfer function. As the chip is manufactured in large batches, all the characteristics of the sensor are given as a statistical study of the sensors. This means that the data sheet does not give the specific range, sensitivity, output data rate, etc. of a given chip, but a range of possible values with a given probability. For example, the sensitivity of the X and Y axes is 2.5 μT/LSB$_{16}$ with an uncertainty of $\pm$8% [17]. Then, the values for the magnetic flux density in each axis given by an Arduino code do not correspond to the real values, but to the ones that would be measured by a chip whose parameters are the typical values shown in the data sheet. Moreover, each Hall sensor has a given offset. The MLX90395 has an offset of $\pm$ 150 LSB$_{16}$ at T$_{amb}$.

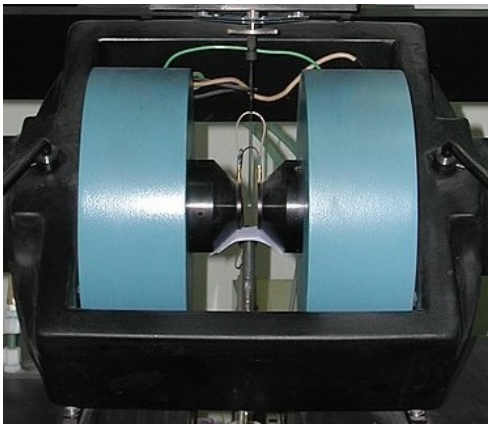

Figure 20: *Vibrating sample magnetometer. The small region between the coils presents a very uniform magnetic field. (Author: Jerôme, Source: https://www.wikiwand.com/en/Vibrating-sample_magnetometer, License: https://creativecommons.org/licenses/by-sa/3.0/)*

To obtain more accurate measurements, we can calibrate the sensor by finding a function that relates the measurements given by the Arduino code to other measurements with lower error. In this case those measurements are provided by a magnetic characterization system: a vibrating sample magnetometer from the general services of magnetic measurements of the Science and Technology Faculty of the University of the Basque Country. The uncertainty of the generated magnetic flux density, in the region where the MLX90395 is placed in order to be calibrated, is of 10^{-3} mT.

To carry out this experiment the MLX90395 is fixed next to the Hall probes situated inside the uniform region of the magnetic field generated by the magnetometer (Figure 20). Then, magnetic fields are generated in the whole measuring range of the Hall sensor and a linear fit is made relating the acquired measurements from the MLX90395 and the ones provided by the magnetometer (Figure 21).

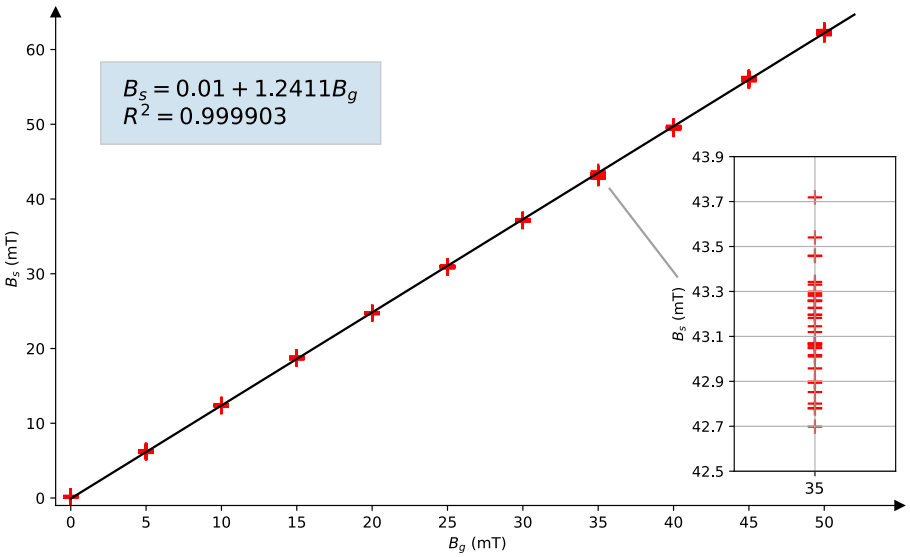

Figure 21: *Linear fit of the sensor magnetic flux density B_s versus the generated B_g. For each generated B_g there are 50 measurements of the sensor B_s, they can be appreciated in the magnified piece of the graph.*

The fit shown in Figure 21 gives the following transfer function for the magnetic flux density of the sensor (B_s)

$$B_s = (0.01 \pm 0.01) + (1.2411 \pm 0.0004)B_g \quad (mT) \tag{1}$$

From where the generated field (B_g), the quantity known to be nearer to the real value, can be isolated and its error computed [23].

$$B_g = \frac{1}{1.2411}(B_s - 0.01) \qquad \Delta B_g = B_g \left[\left(\frac{\Delta B_s + 0.01}{B_s + 0.01} \right)^2 + \left(\frac{0.0004}{1.2411} \right)^2 \right]^{1/2} \quad (mT) \tag{2}$$

This experiment has allowed to eliminate the bias errors in the transfer function of the Hall sensor, the offset and the sensitivity error. The error computed with equation (2) is 0.05 mT along the whole range (0-50 mT), given ΔB_s= 0.04 mT. ΔB_s is computed through the standard deviation of the multiple measurements for each value of B_g.

An interesting realization when making this characterization was that the sensor allowed to measure in a higher range than specified in the data-sheet. And the linearity error increases slowly. This means that if needed, and if precision was not a priority, the MLX90395 medium field sensor could be used to measure in a broader range of magnetic flux density fields.

It is important to mention that this calibration has only been made for the Z axis, which was the most convenient to introduce into the magnetometer. As the chip comes calibrated from the manufacturing company it is an acceptable assumption that all three axes behave in a similar manner. However, it would have been positive to calibrate all three axes independently.

5.2 Synchronization of movement and magnetic measurement

The previous experiment has considered the measurement of a magnetic field independent of the position of the sensor. In the following experiment a new dynamic and error source is introduced: the XYZ positioning table.

The set up of this experiment is as follows. Two NdFeB N45 magnetic cylinders are placed in a dipole configuration. They are attached to the same structure as in Figure 18, which is a piece of the outlet of the beam tube in the Linac-7. The measuring system is aligned with the mentioned piece and the sensor is centered in the tube with the probing algorithm (Section 4.4). Finally, the sensor is moved through a line equidistant to both poles of the dipole taking measurements at every certain length.

The parameters that need to be specified in this experiment are the following:

1. The feed rate of the motors.
2. The time delay between movement and measurement.
3. The number of measurements per point of space.

To verify that the measurements correspond to the real magnetic field generated by the dipole a simulation is performed in FEMM [22] (Figure 22).

At first, it was thought that to make an accurate measurement the limiting factor would be the time delay between movement and measurement. By increasing that time the machine mitigates the vibrations generated in the aluminium bar when accelerating and decelerating. However, after some experiments it was concluded that, provided that the feed rate is below 200 mm/min, the most important parameter is the number of measurements taken in each point. Averaging over a big sample (e.g., 200) eliminates more noise than increasing the time between movement and measurement. The result of these measurements is shown in Figure 23.

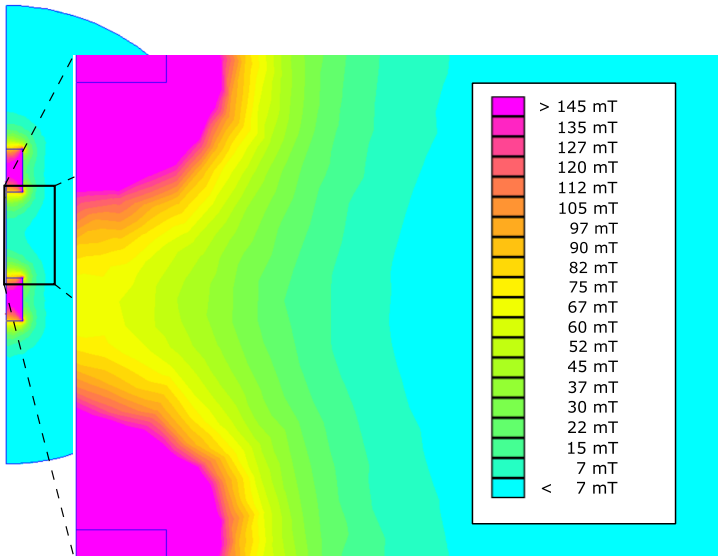

Figure 22: *Simulation in FEMM of the magnetic flux density field generated by the dipole. FEMM has a library which includes the characteristics of the NdFeB N45 permanent magnet. The field is measured in the horizontal line passing through the centre between both magnets.*

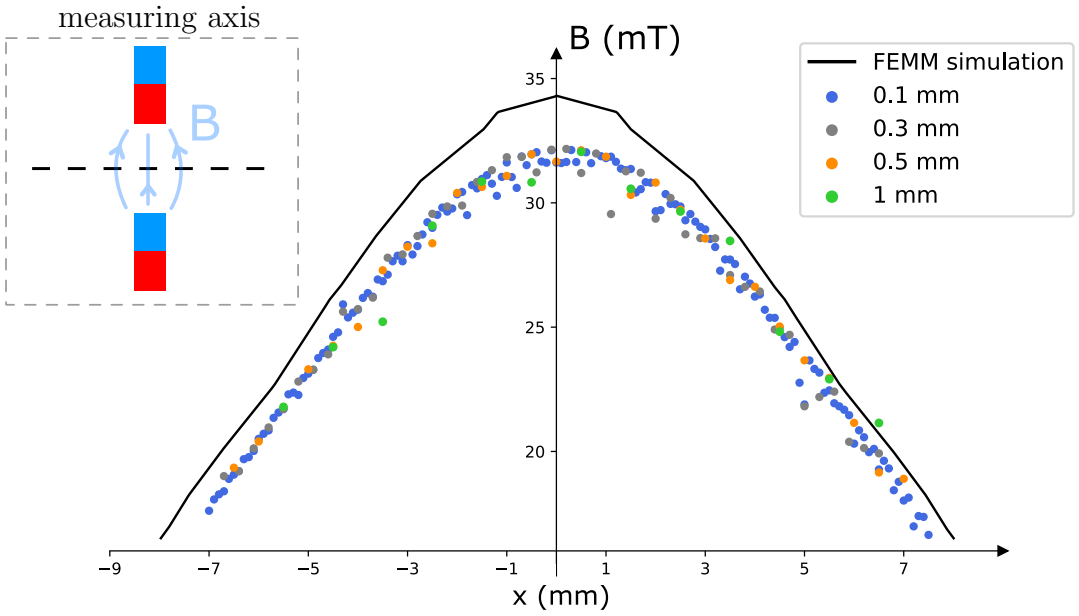

Figure 23: *Magnetic flux density module along an axis equidistant to both poles of a magnetic dipole, a visual scheme is included. Measurements are taken with different spacing: 1 mm, 0.5 mm, 0.3 mm and 0.1 mm. The continuous line is calculated with a simulation performed in FEMM.*

There is a discordance between simulation and measurement. However, that difference comes from the imprecision in setting up the simulation. The real dipole is not perfectly aligned, its magnets are taped with kapton to the outlet piece of the beam tube. Also,

the magnets are simulated as two long magnets, but are actually made up from 3 smaller magnets each and, finally, there can be slight differences between the material defined in FEMM for the NdFeB N45 and the real one.

All in all, the results of this experiment have been satisfactory. The measurements with different spacing all follow the same profile of magnetic flux density. The purpose of this experiment was to find a valid measuring configuration for the XYZ positioning table: a feed rate of less than 200 mm/min and 200 measurements per point in space. The time delay between movement and measurement only has to be enough in order to take the measurements when the machine is at rest.

It can be seen how introducing the movement of the XYZ positioner introduces an important limitation to the characterization of any system: the measurement time. In order to make correct measurements the feed rate of the steppers has been limited and the measurements per point in space set at a minimum value of 200. These factors affect the time it takes to characterize a magnetic field and it will be studied for the particular case of the LEBT characterization in Section 6.

5.3 Mapping of a magnetic quadrupole

This final experiment shows the limitations this system has to measure the magnetic field near the inner wall of a cylinder. The setup is similar to the one in the previous experiment and is shown in Figure 25a. In this experiment, however, the sensor will follow a trajectory such that it measures in a circle with a rectangular grid (Figure 24). This same trajectory is the one it will follow when measuring the magnetic field of the LEBT's solenoid. As the movements in this trajectory are not all of the same length, the time delay between movement and measurement is adapted in each step. That time is estimated from the distance the machine travels, the feed rate and a plus for the accelerating and decelerating intervals (the feed rate is not constant through a given movement).

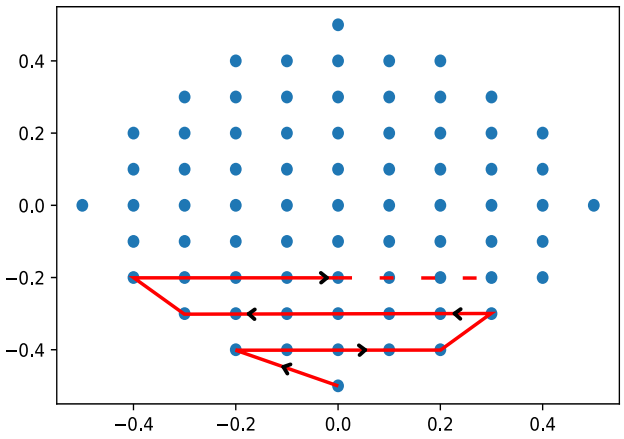

Figure 24: *Mesh (blue points) and the trajectory of the sensor (red line) when measuring a circular region of space.*

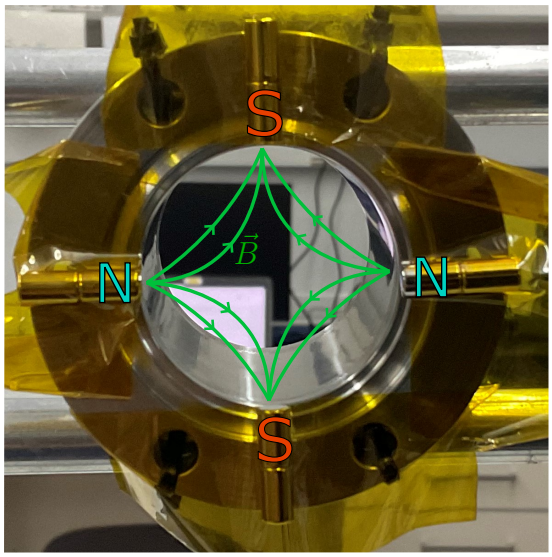

(a) *Quadrupole configuration attached to a beam tube outlet piece of the Linac-7. The poles of the magnets are specified and an scheme of the magnetic field lines is included.*

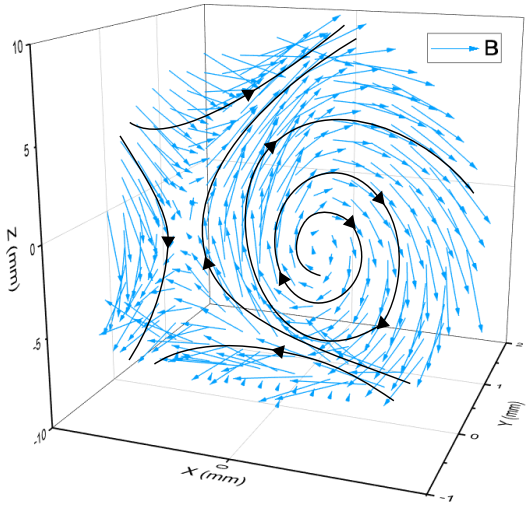

(b) *Experimental mapping of the magnetic flux density of the quadrupole in the plane of the magnets. The black lines scheme the measured magnetic field lines.*

Figure 25: *Measurement of the magnetic flux density field of a quadrupole.*

As can be seen in Figures 25a and 25b these measurements do not seem to follow the natural behavior of a quadrupole. The main reason is that the strength of these magnets is not enough to create the typical well defined quadrupole field. Thus, the characteristic shape of the quadrupole field would only be seen if the measurements were taken very near to the magnets. That kind of measurements are not possible with this system due to the bulkiness of the aluminium bar, whose section is 10×10 mm. However, it can be seen in the left side in Figure 25b a behavior that resembles that of a quadrupole. This is because in that measurement it was tried to get the sensor as near as possible to the magnet on the left side.

With this experiment it is shown that the bulkiness of the aluminium bar does not allow to measure the magnetic field density near the wall of a cylinder. Therefore, it will not be possible to study the border effects of the magnetic field of the LEBT's solenoids. This is not a problem in finding the magnetic axis of the solenoids, but is an impediment in comparing the measured and simulated magnetic flux density fields.

6 Solenoid measurements, data analysis and results

This section describes the procedure followed to construct the magnetic flux density field map of the solenoids which constitute the LEBT. The initial idea was to characterize both solenoids separately. However, the solenoids were set in the structure of the Linac-7 before the characterization could be performed and, therefore, one of the solenoids was inaccessible. Thus, the characterization is made only for one of the solenoids. This is a drawback, but both solenoids are manufactured identically, so it is reasonable to suppose that they have a similar magnetic field.

6.1 Design of the experiment

First, the size and precision of the mesh in which the magnetic field is measured has to be decided. The size of the mesh comes limited by the diameter of the beam tube (38 mm) and the size of the aluminium bar (10 mm × 10 mm). This leaves space to make circles of, in principle, 23 mm in diameter. Nevertheless, for security the trajectories traced will be narrower. To choose the precision of the mesh the limiting factor is the time it takes to make the measurements. An approximate formula for the time it takes to perform a whole measurements is given by

$$t = T_{\text{measurement}} \cdot N_{\text{points}} = \left(t_{mov} + \frac{N_m}{ODR} \right) \cdot \frac{\pi R^2}{\text{precision}^2} \cdot \frac{L}{\text{precision}} \tag{3}$$

where $T_{measurement}$ is time per measurement, N_{points} the number of points in the mesh, t_{mov} the average movement time between point and point, N_m the number of measurements taken in each point, ODR the output data rate of the Hall sensor, R the radius of the mesh, L the length of the solenoid and precision the distance between points. The $\text{T}_{\text{measurement}}$ is of approximately 0.5 s. If a radius of 10 mm is taken and the length of the solenoid, $L = 171$ mm, the total time is of $t \simeq 25 \cdot 10^3/\text{precision}^3$ s. If, for example, the precision is taken to be the minimum distance the positioning table can travel (0.1 mm), the measuring time is greater than two years long. Even if the precision is lowered to 1 mm, the measuring time is 7 hours.

A reasonable measuring time is considered to be under 2 hours. In order to achieve it, the experiment is divided into two different measurements:

1. The first measurement consists in taking measurements in circular sections, as was planned, but only in strategic sections of the solenoid: in the planes where the steel casing begins and ends, and in three locations of each sub-coil, start, center and end. These planes add up to 24, which are then reduced to 19 due to a limitation in the accessible travel for the XYZ positioner when positioned in the LEBT, resulting in a measuring time of around 50 minutes. An scheme of the relevant planes is represented in Figure 26.

2. A second measurement is performed to obtain the magnetic flux density profile of the solenoid along its mechanic axis. This measurement can be made with higher precision, i.e., one point every 0.5 mm, resulting in 3 minutes of measurement. It is a quick experiment which provides a very characteristic feature of the magnetic field of the solenoid.

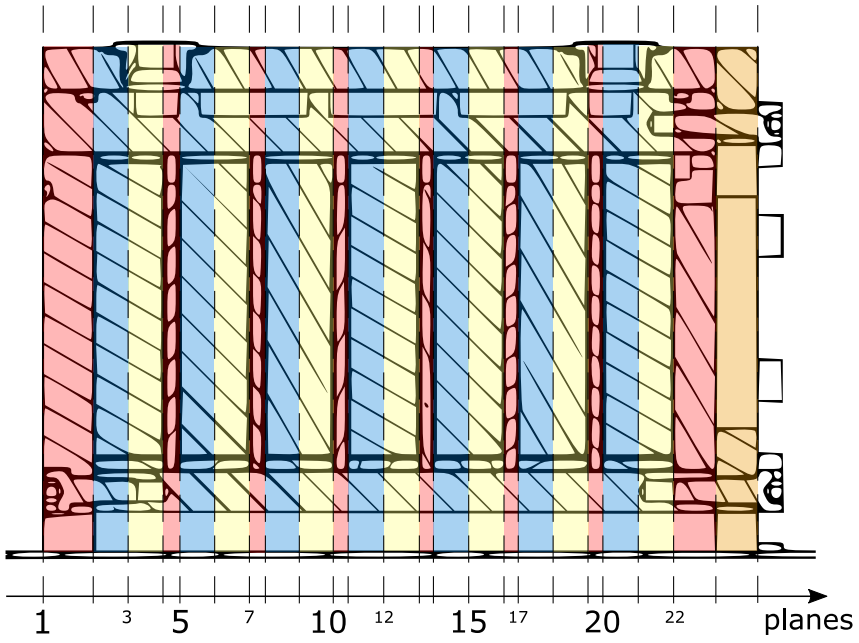

Figure 26: *CAD plane of the solenoid. The relevant planes for the first type of measurements are marked.*

With these two measurements both objectives (Section 1.4) can be fulfilled. From the magnetic flux density contours in 19 planes, distributed over the whole length of the solenoid, the minimum B point in each plane can be obtained and, so, the magnetic axis can be specified. On the other hand, the measurement of the magnetic profile along the axis gives enough information about the field in order to recreate it in simulation.

6.2 Calibration of the system

The relevance of a correct calibration of the system has already been commented in Section 4.5. To set an example of its importance, if the arm of the sensor has a missalignment of 1° with respect to the beam tube, when trying to move the machine from one end of the solenoid to the opposite, it results in an error of 3 mm.

The metrology loop discussed in Section 4.5 sets the parts of the system which need to be properly aligned. First, the aluminium structure which holds the whole system is positioned in front of the Linac-7 (Figure 27). It is adjusted in order to fix the XYZ table at an adequate height. Next, the tilt of all the different parts is adjusted with the bubble level tool. The alignment in the horizontal plane is adjusted by measuring the distance between the structure and the table where the accelerator is set in two different positions. If they are aligned, the distance between structure and table are the same along the whole edge of the table. The distance is measured with a conventional ruler, the precision is 1 mm.

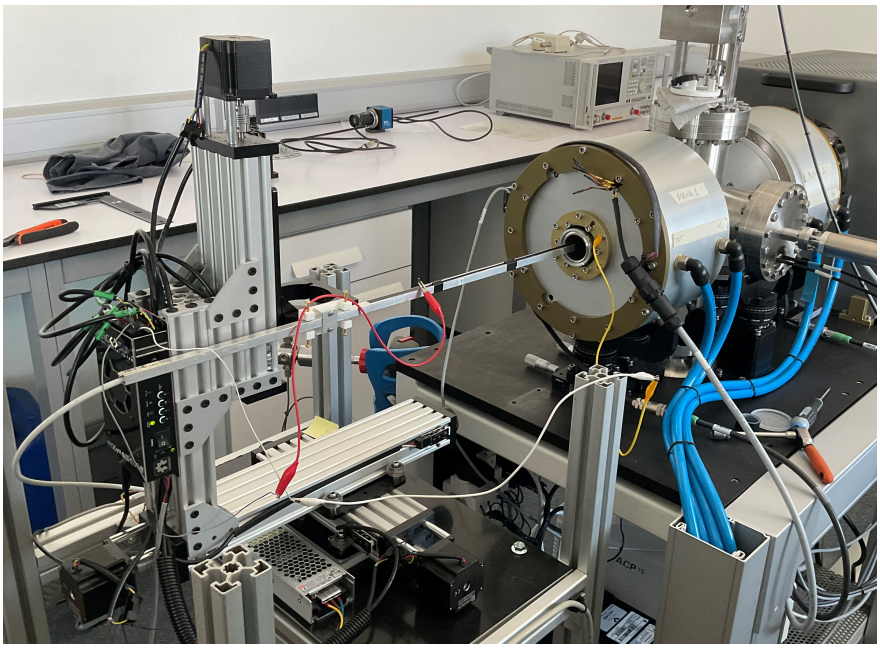

Figure 27: *Setup of the experiment for the characterization of the magnetic flux density field of the solenoid.*

These adjustments serve as a first approximation. To ensure that the aluminium bar which holds the sensor is aligned with the beam tube, the following procedure is followed:

1. The tip of the aluminium bar is set at the start of the beam tube. Then the distance between a face of the bar and the wall of the tube is measured with a caliper.

2. The aluminium bar is introduced a fixed distance into the beam tube (140 mm in this case). The same distance as in step 1 is measured.

3. From the difference between the measurements in steps 1 and 2 it can be known in which direction is the bar tilted. A small adjustment is performed and the procedure is repeated until the difference between both measurements is as small as the conditions allow.

This procedure is followed for the two faces of the aluminum bar. When making measurements in the top face, the corrections are performed through the leveling system incorporated in the 3D printed piece. This allows to align the bar to a difference under 0.1 mm in both measurements, that is, an uncertainty of 0.1°. On the contrary, the system has no integrated system to correct the tilt in the horizontal plane. When measuring distances in the side faces of the aluminium bar, the least difference achieved was of 1 mm. This means that the positions in the X axis will have an error of (y/140) mm, where y is the distance the tip of the bar has traveled inside the tube. This error is a bias error.

In conclusion, with the procedures presented in this section it is ensured that the positions recorded by the software correspond, with a known uncertainty, to the real positions of the sensor within the beam tube. That uncertainty is given by the bias error in the alignment and the precision of the XYZ positioning table.

6.3 Measurements

In this section, the results of the measurements of the magnetic field of the solenoid are presented. They are divided in two iterations. The first iteration will focus in finding the magnetic axis of the solenoid to correct the tilt of the solenoids by means of the instrument shown in Figure 28. Once the magnetic axis is aligned in the second iteration the complete characterization is performed. The results of the second iteration are the ones compared with the simulation in order to examine the validity of the design.

Figure 28: *Micrometric adjusting support of the solenoids.*

6.3.1 First iteration

Contours

In Figure 29 a sample of the magnetic flux density field contours in 4 different XZ planes of the solenoid is shown. From each of the sections the minimum B field point is extracted to reconstruct the magnetic axis of the solenoid.

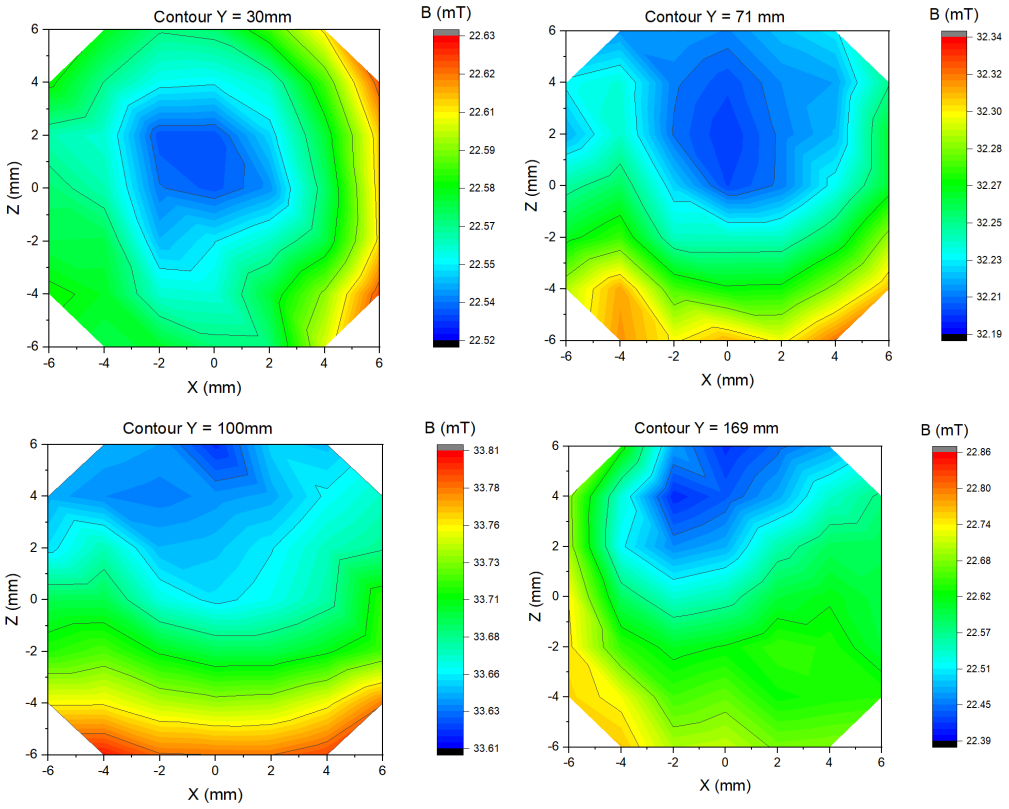

Figure 29: *Magnetic flux density field contour in four XZ planes along the solenoid.*

The projection of the points extracted from the sections is shown in Figure 30. It can be seen how in the XY plane the axis is completely aligned. However, the YZ plane is tilted. In fact, the magnetic axis is not completely inside the region in which the measurements have been taken. That is why the z coordinates of the magnetic axis are constantly 6 mm from $y \simeq 100$ mm onwards.

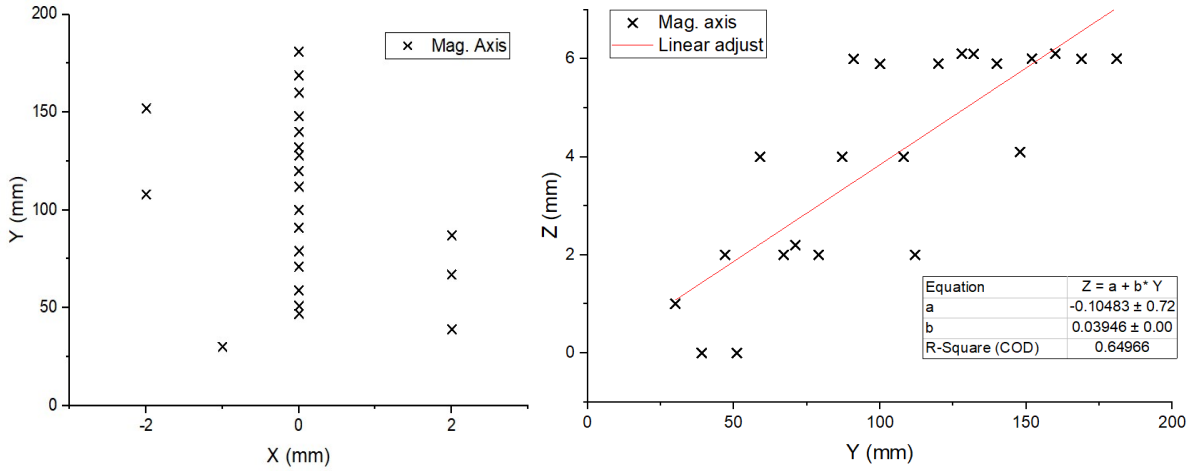

Figure 30: *Coordinates of the measured points along the magnetic axis projected over the XY and YZ planes.*

From the fit in Figure 30 an approximation of the tilt angle of the magnetic axis can be extracted. The fit is really poor due to various reasons: the low number of points available and the saturation experimented by half of them at 6 mm. Also, the figure is misleading because of the difference in scale between the axes. The fit could have been done eliminating the saturated values, but it was preferred to compute a lower value of the tilt and make more iterations if needed. The measured angle is of 2°. With this approximation the tilt of the solenoid is corrected with the micrometric adjust shown in Figure 28.

6.3.2 Second iteration

Contours

The process is repeated and a sample of the results is shown in Figure 31. It can be noticed that the radius of the cylinder has been diminished to 8 mm in order to reduce the measuring time. In this iteration no tilt can be extracted from the data, the points are evenly distributed between $(x = 0, z = 3)$ and $(x = 0, z = 4)$. It can also be be seen that the differences in the magnetic flux density module are of 10^{-2} mT. This is the order magnitude of the error of the Hall sensor (0.05 mT), so making a more accurate measurement of the magnetic axis is beyond this system's capabilities.

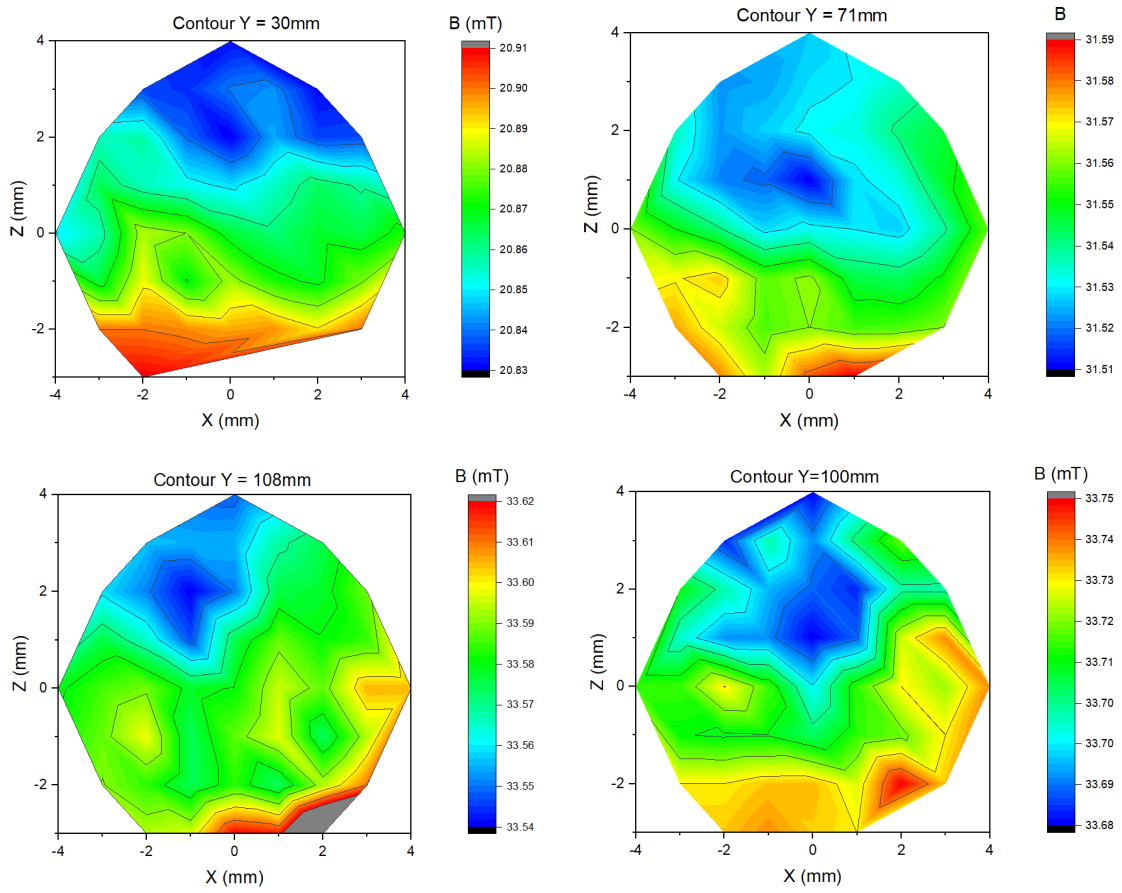

Figure 31: *Magnetic flux density field contour in four XZ planes along the solenoid.*

These two iterations are considered to be sufficient for the purpose of this project. It has been confirmed that the magnetic contours follow the expected behavior of a solenoid and it has been aligned so as to have the region of lower magnetic flux density module parallel to the beam tube.

Magnetic profile along the axis

With the magnetic axis aligned to the beam tube the magnetic profile along the axis can be examined. The purpose of this measurement is to compare it with the simulations performed in Ansys AIM.

The predicted magnetic profile along the axis is shown in red in Figure 32. It can be seen that it does not fit the experimental data. The experimental measurements inside the solenoid are considerably lower than expected and the decay of the field outside the solenoid slower. The green line is the magnetic profile expected for a design with the same geometry as the real design, but changing the number of turns in each of the sub-coils of the solenoid. The reported number of turns by the manufacturer is of 580. In order to obtain the green profile the number of turns in each sub-coil is, from one end to the other: 350-390-490-600-490-390-350. A small variation in the number of turns is expected, because the wire is winded manually. However, the change in the number of turns needed in order to make the simulation match is much higher that what the imprecision of the

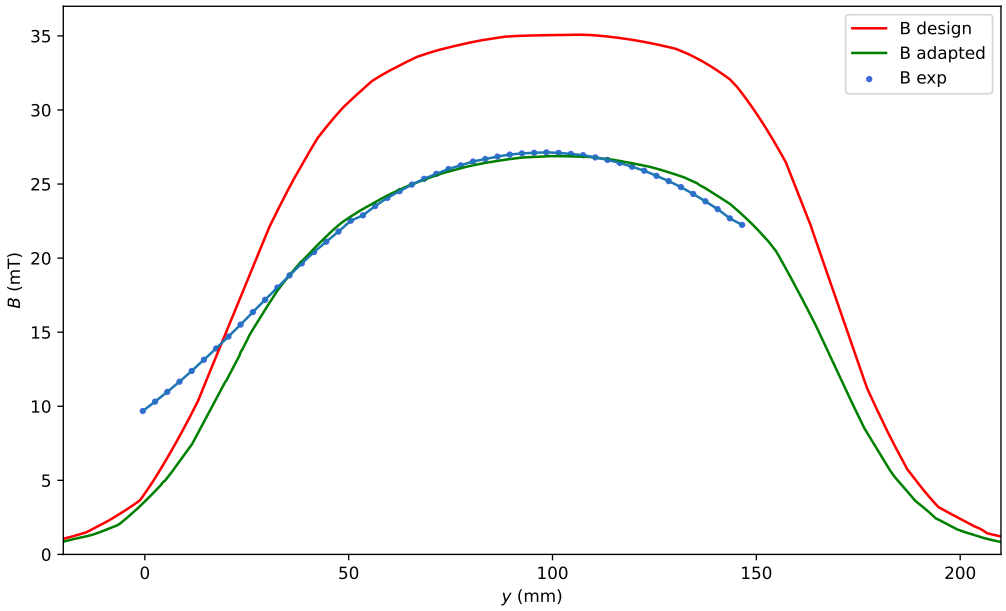

Figure 32: *Magnetic flux density module profile along the magnetic axis of the solenoid. Three curves are shown: the experimental data, the simulation in Ansys of the designed solenoid and an simulation of an adapted design to match the experimental data. Position $y = 0$ marks the start of the solenoid.*

manufacturing process could introduce. Besides, the match between the adapted design and the experimental is not complete, the tails of the profile do not coincide.

In order to find the origin of this mismatch a qualitative comprehension of how the different factors affect the magnetic field of the solenoid is needed. It has already been studied whether the cause is the distribution of the wire through the sub-coils, and it is not. Another factor could be how the current is introduced in the system. The sub-coils are connected in series and the current source is current controlled, which means that the current is the same across the whole solenoids and very stable in the selected value. The final factor that affects the magnetic field is the confinement through the steel casing. The confinement could be reduced because of two reasons: a reduction in the magnetic permeability of the steel and geometric changes in the casing.

The magnetic confinement is what makes the field to decrease rapidly in the region outside the solenoid. Thus, the long tails that present the experimental measurements are indicative of a deficient confinement. The magnetic permeability of the steel can be diminished when it is mechanized. However, it was checked that not even substantial changes in the B-H curve shown in Figure 11 corresponded to profiles such as the measured one. Therefore, the only remaining possibility is a geometry discrepancy between the solenoid design and the manufactured solenoids. For example, a reduction of the width of the caps in the bases of the solenoid of 2 mm would make the material to saturate when operating at 8 A, changing considerably the resulting magnetic field.

Finally, it was found that there is a flaw in the manufacture of the solenoids. The

aforementioned caps of the solenoids were meant to be built with ST-52, the material selected for the casing, but, due to a misunderstanding, they have been built from aluminium, a non-magnetic material. This results in a very poor confinement, the magnetic field lines spread outside the solenoid. The simulation is, then, repeated subtracting the caps of the magnetic confinement and the result is shown in Figure 33.

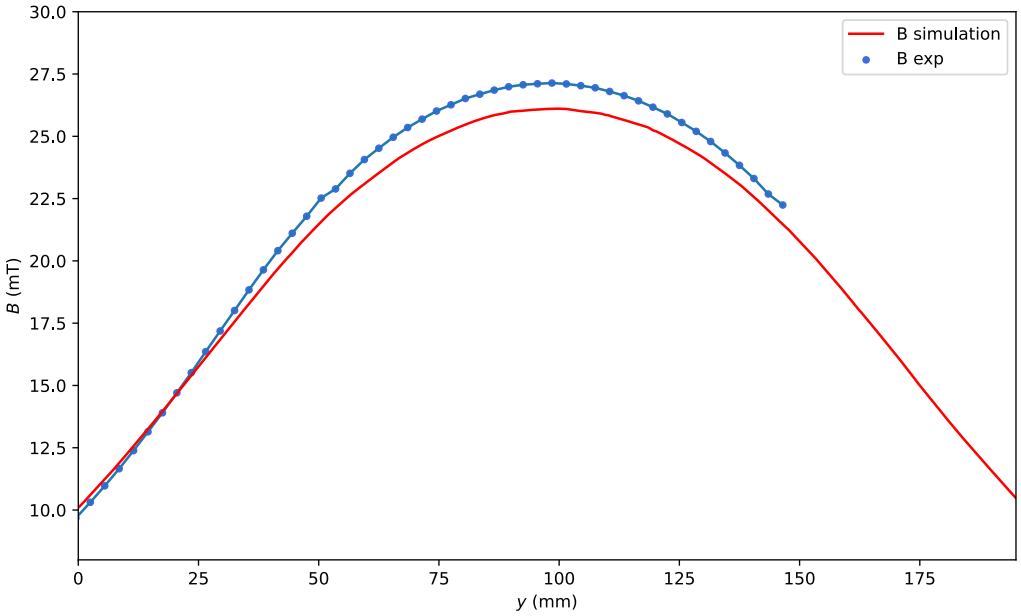

Figure 33: *Magnetic flux density module profile along the magnetic axis of the solenoid. Two curves are shown: the experimental data and the simulation of the solenoid with the defective steel casing. Position $y = 0$ marks the start of the solenoid.*

In Figure 33 both, measurements and simulation, present the same behavior and are very similar to one another, with a maximum difference of 1.03 mT. The discrepancy, now much lower, could have the same origins as stated before: decrease of permeability, difference in the number of turns, etc.

6.4 Further measurements

In addition to the experiments detailed in this section, further measurements where performed. For example, a new trajectory was programmed for the XYZ positioning table in which it performed a cross-like movement in different sections along the Y axis. Also, the magnetic flux density profile along the axis of the beam tube was not only taken for the mechanical axis, but also for different positions along the Z axis. These experiments confirmed the homogeneity of the field along the magnetic axis, but provided no additional information.

7 Conclusions

In this project the solenoids that constitute the LEBT of the Linac-7 have been characterized. For that purpose, a measuring system consisting in a Hall sensor and an XYZ positioner has been designed and assembled. Then, a magnetic flux density field map has been measured and analysed. The most relevant aspects and results of this process are enunciated hereafter. For clarity, it is reported that everything described from Section 2 onwards, except the selection and purchase of the OpenBuilds Minimill, has been carried out by the author.

After making a magnetic field study of the solenoid through simulation in Ansys AIM, a three axis Hall sensor has been selected and implemented. It has been chosen to be accurate and compact. Then, an XYZ positioner has been adapted and programmed to position the sensor at any desired location in space. The whole system, sensor plus XYZ positioner, has been tested through three different experiments: a calibration with a vibrating sample magnetometer and synchronization of movement by measuring a magnetic dipole and quadrupole. The error of the magnetic measurements has been estimated to be 0.05 mT in the range from 0 to 50 mT. The positioning and alignment of the measuring system are also a source of error.

For the characterization, the measuring system was aligned with one of the solenoids of the LEBT through implemented alignment functionalities. Finally, the magnetic flux density vector field of the solenoid is measured with a current of 1 A. By analysing the collected data, the objectives of the project are fulfilled: the magnetic axis has been found and aligned to the beam tube, and the measured magnetic flux density module along the magnetic axis has been compared with simulation.

Due to the magnetic characterization, a manufacturing flaw has been found in the Linac-7's LEBT. Part of the confining steel casing has been built from aluminium instead of ST-52 steel. This results in a bad confining of the magnetic field: the amplitude of the field is lower inside the solenoid and it extends over the outer region of the solenoids. However, taking that into account, simulations and experimental measurements coincide with a maximum discrepancy of 1.03 mT.

This project combines many aspects of electronics, programming and experimental techniques which are reflected in the variety of tools employed: software (Ansys AIM, FEMM, ImageJ, Grbl, Python, Git...), as well as hardware (USB microscope, 3D printer, vibrating sample magnetometer...). The combination of these tools and the competences acquired in the degree have resulted in the presented magnetic field measuring system and the successful characterization of the Linac-7's LEBT.

7.1 Future work

Having found a defect in the manufacturing of the solenoids the next step is clear: replace the aluminium caps in favor of ST-52 caps and repeat the characterization of the solenoids. The result should be similar to that shown in Figure 32.

The designed and assembled magnetic flux density field measuring system has fulfilled its purpose, but could be improved if it were to be used for more generic applications. The improvement proposals are the following:

1. Reduce the size of the aluminium arm that holds the sensor. It has been seen that the 10 mm $\times$ 10 mm section aluminium bar impedes to measure near the sources of the magnetic field (magnets or coils). By implementing the Hall sensor in the QFN-16 package [17], the size of the sensor is reduced to 3mm and the aluminium bar can the be reduced proportionally.

2. Add an alignment functionality in the horizontal plane. The horizontal alignment of the aluminium arm with the beam tube was the most difficult and inaccurate tasks of the alignment process. This problem could be solved installing the measuring system on top of a fine-tuning rotary sliding table

3. Implement a user friendly software to operate the measuring system. An intuitive interface, predefined trajectories of the XYZ positioner and real-time visualization of the measurements could be some examples of its functionalities.

Finally, regarding the design and performance of the LEBT there are some pending tasks. In order to definitely validate the design of the LEBT, its operation has to be checked. The measured magnetic flux density field corroborates the magnetic simulations, which allow to compute the field for any given current of the solenoids. Then, the computed fields can be introduced into an ion optics simulation program in order to select a current that results in the desired focusing of the beam. Finally, experimental measurements of the intensity, trace-space diagram and emittance of the beam will be taken. If the measured characteristics of the beam are compatible with the requirements of the RFQ (the next stage in the Linac-7) the LEBT will be validated.

References

[1] Andrew Sessler and Edmund Wilson, *Engines Of Discovery: A Century Of Particle Accelerators*. Wspc, (2007).

[2] Suzie Sheehy. (2018). "Applications of Accelerators". *Lectures of the CAS-CERN Accelerator School: Introduction to accelerator physics*. Accessed: June 15, 2021. [PowerPoint Slides]. Available: https://indico.cern.ch/event/685255/timetable/

[3] W.T. Weng, S.R. Mane, *Fundamentals of particle beam dynamics and phase space.* Brookhaven National Laboratory Associated Universities, Inc., (1991).

[4] F. Hinterberger, "Lectures of the CAS-CERN Accelerator School: Ion optics with electrostatic lenses." Helmhols-Institut, Univ. of Bonn, Germany, (2006).

[5] O. Meusel, et al., "Low-energy beam transport using space-charge lenses." *Nuclear Instruments and Methods in Physics Research Section A: Accelerators, Spectrometers, Detectors and Associated Equipment*, 544(1–2), (2005).

[6] L. R. Prost, "Selected List of Low Energy Beam Transport Facilities for Light-Ion, High-Intensity Accelerators." *FERMILAB-TM-2622-AD*, (2016).

[7] P. Forck, "Lecture notes on Beam Instrumentation and Diagnostics." Joint Universities Accelerator School (JUAS), 03, (2011).

[8] R. C. O'Handley, *Modern magnetic materials: Principles and applications.* John Wiley & Sons, Inc., Massachusetts Institute of Technology, (2000).

[9] ANSYS, Inc. (1979). Ansys AIM. Accessed: June 15, 2021. [Online]. Available: https://www.ansys.com/

[10] OpenBuilds Design. OpenBuilds Minimill, 3D positioning machine. Accessed: June 15, 2021. [Online]. Available: https://openbuilds.com/builds/openbuilds-minimill.5087/

[11] OpenBuilds Design. OpenBuilds Blackbox, microcontroller. Accessed: June 15, 2021. [Online]. Available: https://openbuilds.com/builds/blackbox-motion-control-system.8320/

[12] Simen Svale Skogsrud, Sungeun(Sonny) K. Jeon. (2009). Grbl. Accessed: June 15, 2021. [Online]. Available: https://github.com/grbl/grbl

[13] ISO 6983-1:2009 Automation systems and integration — Numerical control of machines — Program format and definitions of address words — Part 1: Data format for positioning, line motion and contouring control systems.

[14] S. Sanfilippo, in Proceedings of the CAS-CERN Accelerator School: Magnets, Bruges, Belgium, 16-25 June 2009, edited by D. Brandt, CERN-2010-004.

[15] Terry C. Edwards and Michael B. Steer. *Foundations for Microstrip Circuit Design. Apendix B.* John Wiley & Sons; Fourth Edition, (2016).

[16] Allegro Mycrosystems (2018). ALS31300 Hall sensor data sheet. Accessed: June 15, 2021. [Online]. Available: https://lu.ocean-components.com/datasheet/bf-ALS31300EEJALU-2000.pdf

[17] Melexis (2020). MLX90395 Hall sensor data sheet. Accessed: June 15, 2021. [Online]. Available: https://www.mouser.es/datasheet/2/734/Melexis_MLX90395_Datasheet_Melexis3-1863596.pdf

[18] Multicore (2007). RA 10 SN62BAS86 10K 25G soldering paste data sheet. Accessed: June 15, 2021. [Online]. Available: http://www.farnell.com/datasheets/1683986.pdf

[19] Autodesk, Inc. (1982). Fusion360. Accessed: June 15, 2021. [Online]. Available: https://www.autodesk.es/products/fusion-360

[20] National Institutes of Health (1997). ImageJ. Accessed: June 15, 2021. [Online]. Available: https://imagej.nih.gov/ij

[21] A. Lestrade, in Proceedings of the CAS-CERN Accelerator School: Magnets, Bruges, Belgium, 16-25 June 2009, edited by D. Brandt, CERN-2010-004.

[22] David Meeker. Finite Element Method Magnetics. Accessed: June 15, 2021. [Online]. Available: https://www.femm.info/wiki/HomePage

[23] W. H. Press et al., *Numerical Recipes.* Editorial Cambridge University Press, Cambridge, (1986).